Available online at www.sciencedirect.com
SCIENCE DIRECT®
Icarus 173 (2005) 132–152
ICARUS
www.elsevier.com/locate/icarus

Evidence for asteroid space weathering from the Sloan Digital Sky Survey

David Nesvorný [a,*], Robert Jedicke [b], Robert J. Whiteley [c], Željko Ivezić [d]

[a] *Southwest Research Institute, 1050 Walnut St, Suite 400, Boulder, CO 80302, USA*
[b] *Institute for Astronomy, 2680 Woodlawn Drive, Honolulu, HI 96822, USA*
[c] *Lunar and Planetary Laboratory, University of Arizona, Tucson, AZ 85721, USA*
[d] *Princeton University Observatory, Princeton, NJ 08544, USA*

Received 11 April 2004; revised 29 July 2004

Available online 12 October 2004

Abstract

By studying color variations between young and old asteroid families we find evidence for processes that modify colors of asteroids over time. We show that colors of aging surfaces of S-type asteroids become increasingly 'redder' and measure the rate of these spectral changes. We estimate that the mean spectral slope between 0.35 and 0.9 μm increases with time t (given in My) as $\approx 0.01\ \mu m^{-1} \times \log_{10} t$. This empirical fit is valid only for $2.5 \lesssim t \lesssim 3000$ My (the time interval where we have data) and for the mean spectral slope determined from wide-wavelength filter photometry obtained by the Sloan Digital Sky Survey. We also find that Gy-old terrains of S-type asteroids reflect about 15% more light at ∼ 1-μm wavelengths than an ∼ 5-My-old S-type asteroid surface when the flux is normalized by the reflected light at 0.55 μm. We attribute these effects to space weathering. This result has important implications for asteroid geology and the origin of meteorites that reach the Earth. Our results also suggest that surfaces of C-type asteroids exhibit color alterations opposite to those of the S-type asteroids.

Keywords: Asteroids; Composition; Surfaces; Asteroids; Regoliths

1. Introduction

Studies of soils and rocks collected by the Apollo astronauts provide evidence for processes that alter optical properties of the lunar surface (e.g., Hapke (2001) and references therein). Similarly, optical properties of an asteroid surface change over time (Clark et al., 2002a; Chapman, 2004; and references therein). Because we do not yet have soils taken directly from the surface of an asteroid, surface-aging processes on asteroids are not well understood. Following standard terminology, we will refer to processes that alter optical properties of surfaces of airless bodies (such as solar wind sputtering, micrometeorite impacts, etc.) as 'space weathering' effects.

Two lines of evidence suggest that space weathering effects modify asteroid surfaces:

(i) Although many S-type asteroids are probably similar in bulk composition to ordinary chondrite (OC) meteorites (Gaffey et al., 1993; McFadden et al., 2001; Sullivan et al., 2002), surfaces of S-type asteroids are significantly 'redder' than colors of OC meteorites, and have much shallower olivine/pyroxene absorption band at 1 μm (Chapman and Salisbury, 1973).
(ii) Color variations on surfaces of S-type Asteroids (243) Ida, (951) Gaspra, and (433) Eros mimic the sense of the color differences observed for lunar soils with older surfaces being darker and redder in appearance (Veverka et al., 1996, 2000; Chapman, 2004; Chapman et al., 1996; Clark et al., 2001, 2002a, 2002b; Murchie et al., 2002; Bell et al., 2002). Conversely, it is be-

* Corresponding author. Fax: +1(303)546-9687
E-mail address: davidn@boulder.swri.edu (D. Nesvorný).

0019-1035/$ – see front matter
doi:10.1016/j.icarus.2004.07.026

lieved that other common asteroid types (e.g., the V- and C-types) show little evidence of optical alteration with time (McCord et al., 1970; Veverka et al., 1999; Clark et al., 1999; Keil, 2002).

The rate of change of optical properties by space weathering is poorly understood. Using laser experiments, Sasaki et al. (2001) estimated that micrometeoroid impacts may produce significant space weathering effects on a timescale of order 10^8 years. On the other hand, Hapke (2001) calculated that solar wind sputtering would produce sufficient nanophase iron coatings on regolith grains to account for asteroid space weathering in only 50,000 years. While the micrometeoroid and solar wind bombardment alter optical properties of the uppermost thin layer of regolith, other processes such as the impact blanketing (or tidal 'jolt,' Chapman, 2004) are competing with the above effects to periodically uncover 'fresh,' optically unaltered material (so-called regolith 'gardening'). The resulting surface of an asteroid is a complex product of these processes whose relative importances and relevant timescales are yet to be determined.

Here we use the spectrophotometric data obtained by the Sloan Digital Sky Survey (SDSS) to collect evidence for space weathering on asteroids. We find that the reflectance spectra of S-type asteroids become redder and that the broad absorption band at 1 μm becomes shallower over time. This result is similar to previous observations (references above). We also find indications that surfaces of the C-type asteroids may become bluer over time. If true, then the low-reflectivity material of C-type asteroids exhibits color alterations opposite to those inferred for the higher-reflectivity material of S-type asteroids. We base our evidence on a comparative study of young and old asteroid families[1] that we find by standard techniques but using ten times more asteroid proper elements[2] than previous works (Zappalà et al., 1994, 1995).

Our analysis is in many ways similar to the one used by Jedicke et al. (2004). Here, we add to Jedicke et al.'s results by: (i) augmenting the number of studied asteroid families, (ii) describing in detail our classification of asteroid families and ways their ages were determined, and (iii) examining the effects of space weathering on the 1-μm absorption band.

In Section 2, we describe the photometric system of the SDSS and perform several tests to justify the use of SDSS colors of asteroids. In Sections 3 and 4, we explain how we find asteroid families and how we determine whether an asteroid family is young or old. In Section 5, we show that there exists a correlation between colors and ages of the asteroid families. This result and its implications are discussed in Section 6.

2. SDSS photometry

The recently-released Sloan Digital Sky Survey Moving Object Catalog, hereafter SDSS MOC[3] lists astrometric and photometric data for asteroids observed by the 2.5-meter Sloan telescope located at Apache Point Observatory, in Sunspot, New Mexico. To date, the survey has mapped in detail one-eighth of the entire sky, determining positions, brightnesses, and five-color CCD photometry of 125,283 moving objects (Ivezić et al., 2001; Stoughton et al., 2002).

35,401 unique moving objects detected by the survey (i.e., about 28% of the total) have been matched (Jurić et al., 2002) to known asteroids listed in the ASTORB file (Bowell et al., 1994).[4] The flux reflected by the detected objects was measured almost simultaneously in five bands (measurements in two successive bands were separated in time by 72 s) with effective wavelengths 3557 Å (u band), 4825 Å (g band), 6261 Å (r band), 7672 Å (i band), and 9097 Å (z band), and with 0.1–0.3-μm band widths (Fukugita et al., 1996).

These data provide important and unique information about asteroids because the SDSS MOC includes one to two orders of magnitude more objects than other catalogs that were used in the past to study asteroid visible reflectance spectra. For example, the Small Main-Belt Asteroid Spectroscopic Survey I (SMASS I, (Xu et al., 1995)) and II (SMASS II, Bus and Binzel 2002a, 2002b), which are the largest spectroscopic surveys in visible wavelengths to date, produced a set of visible wavelength spectra for 1447 asteroids. Figure 1 shows a comparison between the total numbers and magnitude distributions of main-belt asteroids observed by the SDSS and SMASS. These two surveys provide complementary information because different magnitude ranges were observed by each of them; the SDSS observed smaller asteroids than the SMASS. The SDSS MOC has been recently used to show many asteroid families segregate in the color space from their local backgrounds (Ivezić et al., 2002), and that this segregation is apparent at least down to absolute magnitude $H \approx 16.0$.

We first verified that the SDSS photometry is consistent with published spectra of asteroids. To this end, we compared the SDSS colors with SMASS spectra [5] for 113 asteroids with known proper elements that appear in both datasets. In 64 cases (i.e., in 57%), the agreement was good (i.e., differences of less then 0.1 in reflectance). To illustrate this, Fig. 2 shows a comparison between the SDSS colors

[1] An asteroid family is a group of asteroid fragments with similar orbits that originated in the catastrophic disruption of a large parent body. Some two dozen robust asteroid families have been identified in the main belt (Zappalà et al., 1994).

[2] The proper elements are analytically defined as constants of orbital motion of a suitably simplified dynamical system. Unlike the instantaneous (i.e., osculating) orbital elements, the proper elements are generally nearly constant on 10^7–10^8 year time scales, and are widely used to decipher the collisional history of the asteroid belt (Milani and Knežević, 1994; Knežević et al., 2002).

[3] http://www.astro.princeton.edu~ivezic/sdssmoc/sdssmoc.html.

[4] ftp://ftp.lowell.edu/pub/elgb/astorb.html.

[5] The SMASS spectra were obtained from http://smass.mit.edu/.

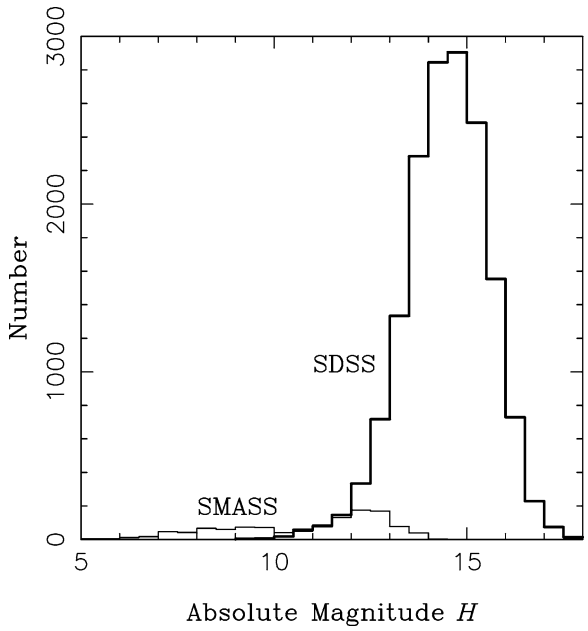

Fig. 1. Absolute magnitude (H) histograms of main-belt asteroids observed by the SDSS and SMASS. Number of observed asteroids in 0.5 magnitude bins is shown. The SDSS magnitude distribution is peaked at 14.0–15.0, where very few SMASS spectra are available. On the other hand, SMASS observed many asteroids with $H < 10.0$. For this reason, the overlap between both datasets is small.

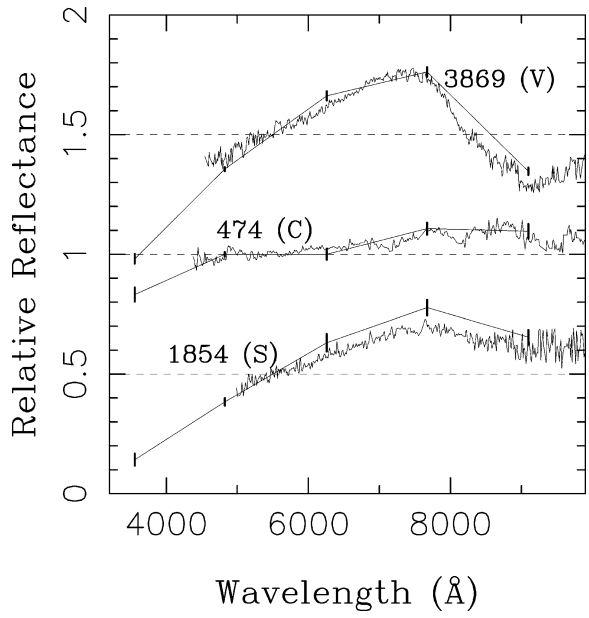

Fig. 2. Comparison between the SDSS band reflectances and the SMASS reflectance spectra for selected S-, C- and V-type asteroids. We subtracted the solar analog from the photometric-calibrated SDSS magnitudes and converted the magnitudes into fluxes. The fluxes were then normalized to 1 at 5500 Å, and offset by 0 or ± 0.5. Vertical segments at 3557, 4825, 6261, 7672, and 9097 Å show 1σ error bars for the SDSS reflectances. (1854) Skvortsov (S-type), (474) Prudentia (C-type), and (3869) Norton (V-type) are shown as examples, where the agreement between the SDSS colors and SMASS spectra was good.

and the SMASS reflectance spectra for selected S-, C- and V-type asteroids. In 43% of cases, the agreement was not as good. In these cases, the SDSS colors follow the global shape of the SMASS spectra, but either show systematically a slightly steeper slope, or the reflectance in the z band (9097 Å effective wavelength) does not drop as much as the SMASS spectrum near the 1-μm absorption band. Individual SDSS measurements of the flux may differ by as much as 10–20% from the values measured by the SMASS.

The origin of these differences cannot be explained by the accuracy of the SDSS and/or SMASS observations. Repeated observations of the same sources demonstrate that the spectrophotometric accuracies of the SDSS and SMASS are ~ 0.02 and ~ 0.01 mag, respectively (Ivezić et al., 2003; Bus and Binzel, 2002a), which accounts for only a small fraction of the observed discrepancy. The effect of phase reddening on the SDSS colors is also unlikely to cause a difference because the SDSS observed at low phase angles ($\approx 7°$ rms, $\approx 35°$ maximum). Errors in the SDSS colors generated by calibration, atmospheric extinction, etc., are also small ($\lesssim 0.2$ mag). Similarly, great care was taken in calibrating the SMASS observations (Bus and Binzel, 2002a).

We explain the discrepancy between the SMASS spectra and the SDSS colors by the wavelength range of the SDSS filters. In Fig. 2, the SDSS color values were plotted at the effective wavelengths of the SDSS filters (Fukugita et al., 1996). It is not correct to compare these values with the SMASS reflectance spectra at the same wavelengths, because the SMASS values are local, narrow-wavelength-range spectral reflectances while the SDSS filters integrate the reflectance spectra over their 0.1–0.3-μm band widths. To test this explanation, the SMASS spectra should be convolved with the SDSS filters and only then be compared to the SDSS colors. Unfortunately, this cannot be done because the SDSS filters span a larger wavelength range than the SMASS data (~ 0.3–1.2 μm compared to SMASS's ~ 0.45–1.0 μm) with only the central SDSS's r and i bands being located within the range of SMASS wavelengths.

To verify whether or not these differences may compromise our analysis, we have performed several tests. The SMASS data provided a basis for developing a new asteroid taxonomic system (Bus and Binzel, 2002b) that classifies reflectance spectra into a few categories that have interpretations in terms of the surface mineralogy of asteroids. For example, the S-type taxonomic category is characterized by a spectral redness that is usually attributed to the reflectance properties of Fe/Mg-bearing silicates such as olivine and pyroxene. We may thus ask whether the five-color SDSS photometry is good enough to distinguish between asteroids of different taxonomic types.

We utilize an algorithm that automatically analyzes photometric data in the SDSS MOC and classifies asteroids according to their taxonomic types. This algorithm uses the Principal Component Analysis (hereafter PCA). The PCA involves a mathematical procedure that transforms a number of possibly correlated variables into a smaller number of uncorrelated variables called principal components. The first principal component accounts for as much of the variabil-

ity in the data as possible, and each succeeding component accounts for as much of the remaining variability as possible. In the result, the PCA creates linear combinations of the five SDSS colors that maximize the separation between the taxonomic types in the SDSS data.

The first two principal components (i.e., the new uncorrelated variables) that this algorithm yields are given by the following relationships[6]

$$\begin{aligned}\mathrm{PC}_1 &= 0.396(u-g)+0.553(g-r)+0.567(g-i)\\ &\quad +0.465(g-z),\\ \mathrm{PC}_2 &= -0.819(u-g)+0.017(g-r)+0.09(g-i)\\ &\quad +0.567(g-z),\end{aligned} \tag{1}$$

where u, g, r, i, z are the measured fluxes in five bands after correction for solar colors. To illustrate the result of the PCA, Fig. 3 shows the principal components (Eq. (1)) of ~ 100 asteroids with previously known taxonomic types (Bus and Binzel, 2002b) that were detected by the SDSS. This figure demonstrates that we can use the first two principal components to distinguish taxonomic complexes such as S, C, or X (see Bus and Binzel (2002b) for their definitions); indeed, these complexes occupy different locations in the $(\mathrm{PC}_1, \mathrm{PC}_2)$ plane.[7] S-complex asteroids generally have $\mathrm{PC}_1 > 0.35$, C-complex asteroids have $\mathrm{PC}_1 < 0.35$ and $\mathrm{PC}_2 \lesssim -0.1$, X-complex asteroids have $\mathrm{PC}_1 \lesssim 0.35$ and $\mathrm{PC}_2 \gtrsim -0.1$. Moreover, (4) Vesta and V-type asteroids in the Vesta family (see, e.g., Cellino et al., 2002) have $\mathrm{PC}_1 \gtrsim 0.35$ and small PC_2 (only one V-type asteroid was observed by both SDSS and SMASS as shown in Fig. 3: (2704) Julian Loewe has $\mathrm{PC}_1 \approx 0.5$ and $\mathrm{PC}_2 \approx -0.4$).

Based on these results, we conclude that the SDSS MOC is a useful, self-consistent dataset to study general, statistical variations of colors of small asteroids in the main belt but that caution is required to interpret colors in individual cases.[8] In this work, we study systematic color variations within the taxonomic complexes and the correlation of colors with other parameters.

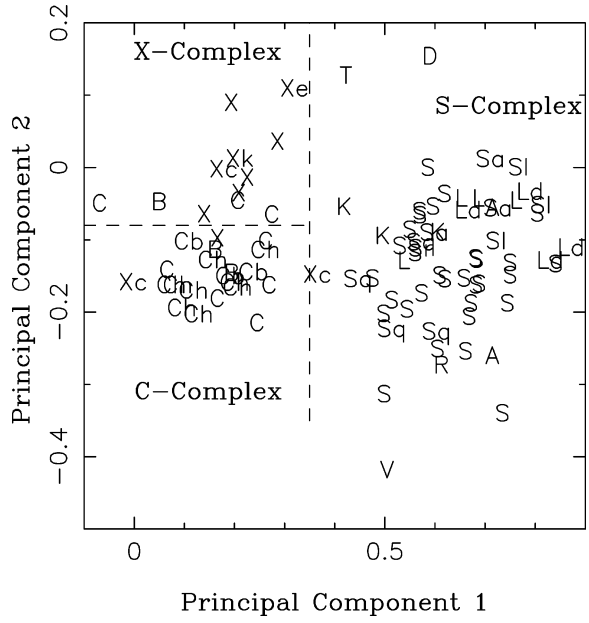

Fig. 3. SDSS asteroids with known taxonomic types shown in the Principal Component Plane. This plot shows PC_1 and PC_2 (Eq. (1)) of ~ 100 asteroids detected by the SDSS that have 0.1 mag or smaller errors in PC_1 and PC_2 and that have been taxonomically classified by Bus and Binzel (2002b). We see that members of taxonomic complexes S, C, and X are located in three different regions (dashed lines schematically delimit these regions). R, K, T, D, L, Ld, A, Sa, Sl, Sq, Sr types are subcategories of the S complex. Similarly, B, Ch, Cb and Xc, Xk, Xe are subcategories of the C and X complexes, respectively (Bus and Binzel, 2002b).

3. Asteroid families

The asteroid belt has collisionally evolved since its formation (see Davis et al., 2002 and other chapters in Section 4.2 of the Asteroids III book). Possibly its most striking feature is the asteroid families that represent remnants of large, collisionally disrupted asteroids (Hirayama, 1918). In the present asteroid belt most asteroid families can be clearly distinguished from the background population of asteroids.

To make an efficient use of the SDSS MOC we want to sort the main-belt asteroids into family and background populations and analyze color variations within these sets separately. The analysis of the asteroid families may tell us about things such as asteroid interiors, geological differentiation in the main belt, or about phenomena that alter asteroid colors with time. The analysis of background asteroids is more related to issues such as the primordial temperature gradient in the proto-planetary nebula, subsequent dynamical excitation and mixing of bodies formed at different orbital distances from the Sun. Here, we concentrate on systematic color variations between the asteroid families.

To identify asteroid families, researchers look for clusters of asteroid positions in the space of proper elements:

[6] This definition of the principal components slightly differs from the one used by Jedicke et al. (2004) because we used a slightly different dataset for the PCA than Jedicke et al. (2004). These differences are insignificant in the context of this study. The PCA produces color components that more rigorously separate asteroid colors than a and i–z color components used by Ivezić et al. (2002). Nevertheless, there exists a correlation between Ivezić et al.'s a and our PC_1, and between Ivezić et al.'s i–z and our PC_2. We will show in Section 5 that PC_1 is a proxy for the spectral slope and PC_2 is related to the spectral curvature.

[7] Each of the three main categories has a number of taxonomic subdivisions depending on the depths of the absorption bands, relative redness or blueness of the reflected light, and other features such as the presence/absence of specific absorption bands (Bus and Binzel, 2002b). Classification into these categories is difficult to achieve with the SDSS photometry because there is usually not enough resolution with only five colors to detect these spectral signatures.

[8] For example, Fig. 3 shows that about 5% of asteroids in the C-complex region ($\mathrm{PC}_1 \leqslant 0.35$ and $\mathrm{PC}_2 \lesssim -0.1$) are not C-complex bodies and that about 2% of asteroids in the S-complex region ($\mathrm{PC}_1 \geqslant 0.35$) are not S-complex type bodies. Also, about 3% of the SDSS MOC entries are instrumental artifacts (Ivezić et al., 2002).

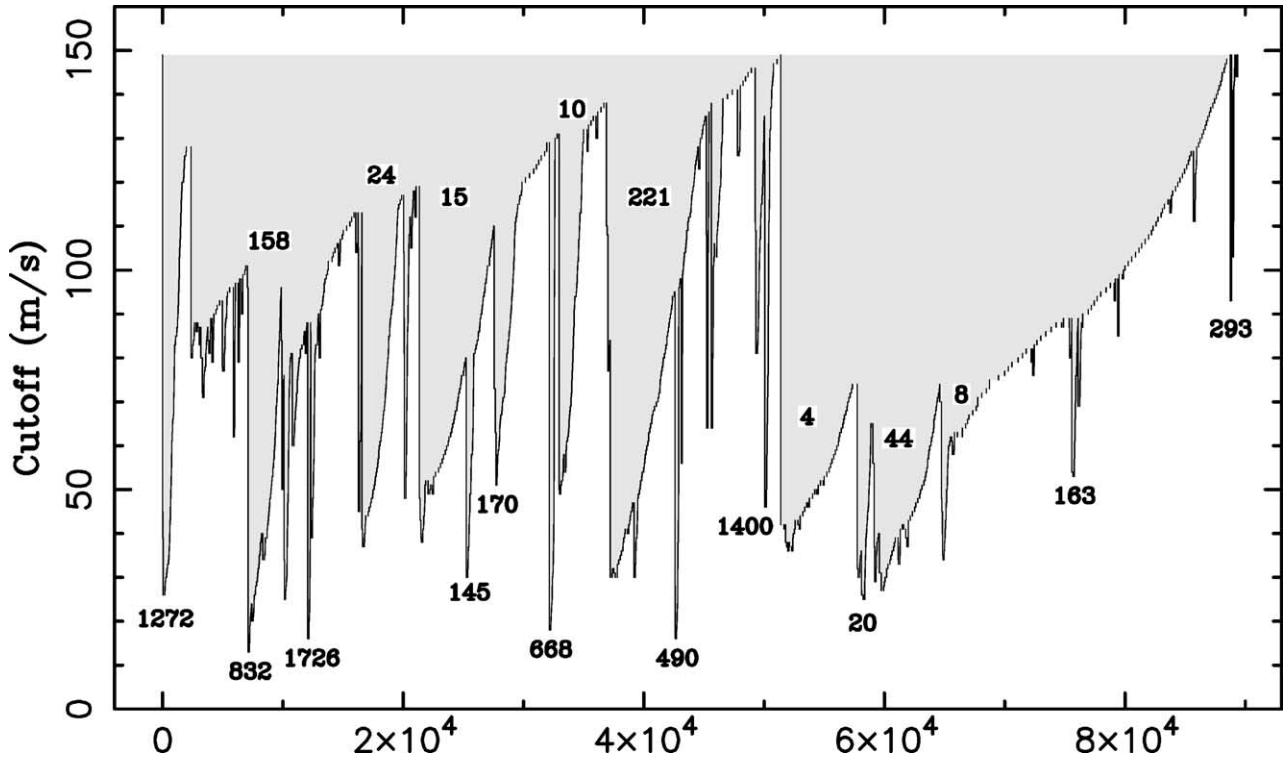

Fig. 4. The dynamical structure of the asteroid belt represented in the 'stalactite diagram.' Each stalactite represents an asteroid family and is labeled by the member asteroid that has the lowest designation number. The width of a stalactite at cutoff $d_{\rm cutoff}$ shows the number of family members that were identified with $d_{\rm cutoff}$. Large families, such as those associated with (158) Koronis, (24) Themis, (15) Eunomia, (221) Eos, (4) Vesta, and (44) Nysa, appear as thick stalactites that persist over a large range of $d_{\rm cutoff}$. Smaller families are represented by thin stalactites that are often (but not always, see, e.g., (490) Veritas) vertically short meaning that their determination requires a specific narrow range of $d_{\rm cutoff}$. About fifty asteroid families are shown in this figure.

the proper semimajor axis ($a_{\rm P}$), proper eccentricity ($e_{\rm P}$), and proper inclination ($i_{\rm P}$) (Milani and Knežević, 1994; Knežević et al., 2002). These orbital elements describe the size, shape and tilt of orbits. Proper orbital elements, being more constant over time than instantaneous orbital elements, provide a dynamical criterion of whether or not a group of bodies has a common ancestor.

To identify an asteroid family, we use a numerical code that automatically detects a cluster of asteroid positions in the 3-dimensional space of proper elements. We based our code on the so-called Hierarchical Clustering Method (hereafter HCM, Zappalà et al., 1990). The HCM requires that members of the identified cluster of asteroid positions in the proper elements space be separated by less than a selected distance (the so-called 'cutoff').

In the first step, we apply the HCM to a catalog of proper asteroid elements (Milani and Knežević, 1994; Knežević et al., 2002).[9] The catalog we used for this work includes 106,284 proper elements (10/10/2002 release). The procedure starts with an individual asteroid position in the space of proper elements and identifies bodies in its neighborhood with mutual distances less than a threshold limit ($d_{\rm cutoff}$). We define the distance in $(a_{\rm P}, e_{\rm P}, i_{\rm P})$ space by

$$d = na_{\rm P}\sqrt{C_a(\delta a_{\rm P}/a_{\rm P})^2 + C_e(\delta e_{\rm P})^2 + C_i(\delta \sin i_{\rm P})^2}, \qquad (2)$$

where $na_{\rm P}$ is the heliocentric velocity of an asteroid on a circular orbit having the semimajor axis $a_{\rm P}$. $\delta a_{\rm P} = |a_{\rm P}^{(1)} - a_{\rm P}^{(2)}|$, $\delta e_{\rm P} = |e_{\rm P}^{(1)} - e_{\rm P}^{(2)}|$, and $\delta \sin i_{\rm P} = |\sin i_{\rm P}^{(1)} - \sin i_{\rm P}^{(2)}|$. The indexes (1) and (2) denote the two bodies in consideration. C_a, C_e and C_i are weighting factors; we adopt $C_a = 5/4$, $C_e = 2$ and $C_i = 2$ (Zappalà et al., 1994). Other choices of C_a, C_e and C_i yield similar results.

The cutoff distance $d_{\rm cutoff}$ is a free parameter. With small $d_{\rm cutoff}$ the algorithm identifies tight clusters in the proper element space. With large $d_{\rm cutoff}$ the algorithm detects larger and more loosely connected clusters. For the main belt, the appropriate values of $d_{\rm cutoff}$ are between 1 and 150 m/s. To avoid an a priori choice of $d_{\rm cutoff}$, we developed software that runs HCM starting with each individual asteroid in our $N = 106,284$ sample and loops over 150 values of $d_{\rm cutoff}$ between 1 and 150 m/s with a 1 m/s step. The code has been optimized so that this job takes only a few days on a fast workstation.

In Fig. 4, we illustrate the final product of this algorithm using a 'stalactite' diagram (Zappalà et al., 1994). For each $d_{\rm cutoff}$ on the Y-axis we plot all clusters found by the HCM. For example, with $d_{\rm cutoff} = 150$ m/s, nearly the whole main belt is linked to a single asteroid, (1) Ceres. We plot a horizontal line segment at $d_{\rm cutoff} = 150$ m/s with length equal to the total number of members in this cluster. At smaller $d_{\rm cutoff}$

[9] Available at the AstDys node, http://hamilton.dm.unipi.it/cgi-bin/astdys/astibo.

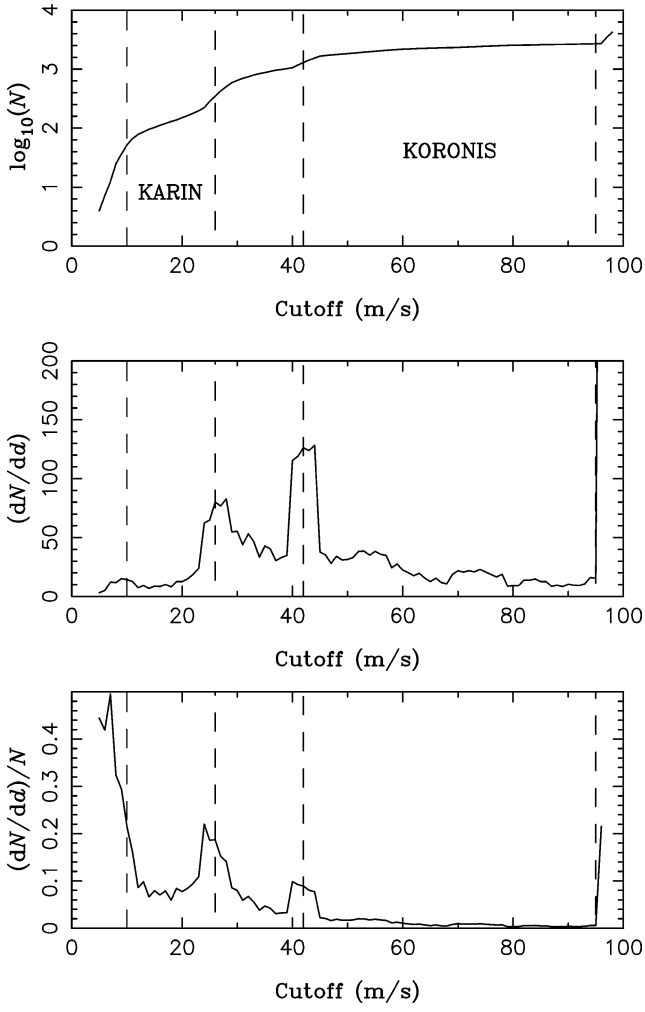

Fig. 5. From top to bottom, the panels show the logarithm of the total number of the Koronis family members $\log_{10}(N)$, the first derivative $\mathrm{d}N/\mathrm{d}d_{\mathrm{cutoff}}$, and $(\mathrm{d}N/\mathrm{d}d_{\mathrm{cutoff}})/N$ to enhance features for small N. The vertical dashed lines indicate d_{cutoff} that correspond to important changes in the slope of $N(d_{\mathrm{cutoff}})$.

the complex structure of the main asteroid belt emerges. The stalactite diagram is extremely useful when we want to systematically classify this information. In fact, more than fifty significant groups are shown in Fig. 4—twice the number of robust asteroid families known previously (Bendjoya and Zappalà, 2002). We label each stalactite by the lowest numbered asteroid in the group (not all these labels appear in Fig. 4), and proceed to the second step of our algorithm.

In the second step, we select appropriate d_{cutoff} for each particular cluster. Unlike the first step of our algorithm that is fully automated, the second step requires some nontrivial insight into the dynamics of the main-belt asteroids, and cannot be fully automated. We illustrate this for the Koronis family (Zappalà et al., 1994). Figure 5 shows how the number $N(d_{\mathrm{cutoff}})$ of members of the cluster linked to (158) Koronis changes with d_{cutoff}. The two bottom panels show derivatives of $N(d_{\mathrm{cutoff}})$ that we use to find values of d_{cutoff}, where $\mathrm{d}N(d_{\mathrm{cutoff}})/\mathrm{d}d_{\mathrm{cutoff}}$ is large (these d_{cutoff} values are labeled by vertical dashed lines). Each of these four d_{cutoff} values has a clear interpretation. To correlate these values of d_{cutoff} with structures and processes operating in the main belt, we generate movies that show projections of the dynamical structure of families into $(a_{\mathrm{P}}, e_{\mathrm{P}})$ and $(a_{\mathrm{P}}, i_{\mathrm{P}})$ planes.[10] Moreover, we programmed an interactive visualization tool that allows us to work in three dimensions thus avoiding problems generated by the projection effects into either $(a_{\mathrm{P}}, e_{\mathrm{P}})$ or $(a_{\mathrm{P}}, i_{\mathrm{P}})$ planes.

With $d_{\mathrm{cutoff}} \lesssim 12$ m/s, the algorithm accumulates members of a very tightly clustered group—the product of a collisional breakup of the Koronis family member about 5.8 My ago (Karin cluster, Nesvorný et al., 2002a). With $d_{\mathrm{cutoff}} \sim 23$ m/s, the HCM starts to agglomerate the central part of the Koronis family. With $d_{\mathrm{cutoff}} \sim 40$ m/s, the algorithm steps over the secular resonance that separates central and large semimajor axis parts of the Koronis family (this particular shape resulted from long-term dynamics driven by radiation forces, Bottke et al., 2001). Finally, with $d_{\mathrm{cutoff}} \gtrsim 95$ m/s, the algorithm starts to select other structures in the outer main belt that have unrelated origins. This can be seen in Fig. 4, where many small stalactites join the Koronis family at $d_{\mathrm{cutoff}} \gtrsim 100$ m/s.

According to these considerations, $d_{\mathrm{cutoff}} = 10$–20 m/s is the best choice for the Karin cluster and $d_{\mathrm{cutoff}} = 50$–90 m/s is best for the Koronis family. For other families, we choose d_{cutoff} using similar criteria. This effort requires human intervention because it is difficult (if not impossible) to program a general algorithm that takes into account all relevant processes operating in the main belt (such as resonances, radiation forces, etc.). A systematic analysis of 50+ clusters required a significant work effort.[11] The final product of our algorithm are the asteroid families (Table 1), lists of their members selected at appropriate cutoffs, and the list of background asteroids showing no apparent groups. Figure 6 illustrates this result: from top to bottom, the panels show all main-belt asteroids, family members, and background asteroids, respectively. From the total of 106,284 main-belt asteroids, 38,625 are family members (36.3% of total) and 67,659 are background asteroids (63.7%).

To determine whether our algorithm produced a reasonably complete list of asteroid families, we searched for residual clusters in the background asteroid population using

[10] http://www.boulder.swri.edu~davidn/morby/NEWfam(100,000PE)/.

[11] To demonstrate the statistical significance of each family we generated synthetic distributions of the proper elements and applied the HCM to them. For example, to demonstrate larger than 99% statistical significance of the Karin cluster, we generated 100 synthetic orbital distributions corresponding to the Koronis family determined at $d_{\mathrm{cutoff}} = 70$ m/s (i.e., 2388 asteroid positions at $2.83 < a_{\mathrm{P}} < 2.95$ AU, $0.04 < e_{\mathrm{P}} < 0.06$, and $0.033 < i_{\mathrm{P}} < 0.04$), and applied our HCM algorithm to these data. With $d_{\mathrm{cutoff}} = 10$ m/s, we were unable to find a cluster containing more than five members, yet the Karin family contains 84 members with this d_{cutoff} (Fig. 5). We also used the HCM algorithm on 100 computer-generated asteroid belts (i.e., 106,284 random orbital positions at $2.1 < a_{\mathrm{P}} < 3.25$ AU, $e_{\mathrm{P}} < 0.3$, and $i_{\mathrm{P}} < 0.3$). Once again, $d_{\mathrm{cutoff}} = 10$ m/s yielded no meaningful structures. We are thus confident that the Karin cluster and other families to which we applied the same technique are statistically robust.

Table 1
List of selected, statistically-robust asteroid families with SDSS color data

Family	d_{cutoff} (m/s)	# of mem.	# in SDSS	Tax. type	PC_1	PC_2	Age (Gy)
3 Juno	50	74	2/11	S	0.523	−0.150	–
4 Vesta	70	5575	372	V	0.491	−0.288	–
8 Flora	80	6131	449	S/C[1]	–	–	1.0 ± 0.5^{d}
10 Hygiea	80	1136	81	C	0.081	−0.170	2.0 ± 1.0^{g}
15 Eunomia	80	3830	387	S	0.624	−0.156	2.5 ± 0.5^{g}
20 Massalia	50	966	36	S	0.493	−0.139	0.3 ± 0.1^{d}
24 Themis	90	2398	208	C	0.092	−0.179	$2.5 \pm 1.0^{a,g}$
44 Nysa(Polana)	60	4744	229	S/F[2]	–	–	–
46 Hestia	80	154	11	S	0.624	−0.151	–
87 Sylvia	60	19	1/2	–	0.137	0.033	–
128 Nemesis	70	133	12	C	0.189	−0.196	0.2 ± 0.1
137 Meliboea	120	57	12	C	0.185	−0.161	–
145 Adeona	60	533	68	C	0.112	−0.189	$0.7 \pm 0.5^{e,g}$
158 Koronis[3]	70	2304	174	S	0.522	−0.111	$2.5 \pm 1.0^{a,c}$
163 Erigone	80	410	22	C/X	0.138	−0.131	–
170 Maria	100	1621	155	S	0.578	−0.107	3.0 ± 1.0^{g}
221 Eos	80	4412	457	S	0.466	−0.104	2.0 ± 0.5^{f}
283 Emma	40	76	8/12	–	0.129	−0.053	–
293 Brasilia[4]	80	95	7/15	C/X	0.222	−0.076	0.05 ± 0.04
363 Padua	70	303	22	C/X	0.273	−0.122	0.3 ± 0.2
396 Aeolia	20	28	2/3	–	0.270	−0.187	–
410 Chloris	120	135	10	C/X	0.241	−0.093	0.7 ± 0.4
490 Veritas	50	284	35	C	0.212	−0.230	8.3 ± 0.5 My^{d}
569 Misa	80	119	8/15	C	0.154	−0.185	0.5 ± 0.2
606 Brangane	30	30	3/5	S	0.441	0.061	0.05 ± 0.04
668 Dora	70	404	35	C	0.091	−0.190	0.5 ± 0.2^{g}
808 Merxia	100	271	16	S	0.455	−0.115	0.5 ± 0.2
832 Karin	10	84	3/6	S	0.387	−0.228	5.8 ± 0.2 My^{d}
845 Naema	40	64	8/13	C	0.135	−0.178	0.1 ± 0.05
847 Agnia	40	252	18	S	0.435	−0.169	0.2 ± 0.1
1128 Astrid	50	65	6/7	C	0.221	−0.210	0.1 ± 0.05
1272 Gefion	80	973	85	S	0.544	−0.123	1.2 ± 0.4^{e}
1400 Tirela	70	212	13	–	0.714	−0.128	–
1639 Bower[5]	100	82	5/10	–	0.528	0.026	–
1644 Rafita	100	382	19	S	0.538	−0.127	1.5 ± 0.5
1726 Hoffmeister	50	235	22	C/X	0.058	−0.115	0.3 ± 0.2^{d}
2980 Cameron	60	162	12	S	0.518	−0.116	–
3556 Lixiaohua	50	97	7/13	C/X	0.170	−0.080	0.3 ± 0.2
4652 Iannini	30	18	0/3	S[6]	0.324	−0.109	$\lesssim 5$ My^{d}
9506 Telramund	60	70	3/9	S	0.502	−0.166	–
18405 FY12	50	11	3/3	X	0.214	0.001	–

The columns are: lowest numbered asteroid family member; cutoff limit used (d_{cutoff}); number of family members determined at this cutoff; number of family members in the SDSS MOC (for small families we list N_1/N_2; where N_1 is the number of family members with 0.1 or smaller errors in PC_1 and PC_2, and N_1 is the number of family members with 0.3 or smaller errors PC_1 and PC_2); common taxonomic-complex types among the family members as suggested by PC_1 and PC_2 (not listed if ambiguous or listed, e.g., as C/X if both C- and X-types are common); the mean PC_1 and PC_2 values; and the age of the family, when available. Sources for family ages are: (a) Marzari et al. (1995, 1999), (b) Durda and Dermott (1997), (c) Bottke et al. (2001), (d) Nesvorný et al. (2002a, 2002b, 2003), (e) Carruba et al. (2003), (f) Vokrouhlický et al. (in preparation), (g) http://www.boulder.swri.edu~bottke/Yarkovsky, and this work if no label appears in the last column.

[1] Dynamical family shows a complex mixture of taxonomic types.
[2] Nysa (S-type) and Polana (F-type; Cellino et al., 2002) families listed together.
[3] The Karin cluster is excluded.
[4] (293) Brasilia is probably an interloper (Nesvorný et al., 2003).
[5] (1639) Bower is probably an interloper (Nesvorný et al., 2003).
[6] Taxonomic type was determined for members with $\delta PC_1 < 0.3$ and $\delta PC_2 < 0.3$.

proper elements and colors simultaneously. We defined the distance in $(a_P, e_P, i_P, PC_1, PC_2)$ space by

$$d_2 = \sqrt{d^2 + C_{PC}\left[(\delta PC_1)^2 + (\delta PC_2)^2\right]}, \quad (3)$$

where d is the distance in (a_P, e_P, i_P) subspace defined in Eq. (2), $\delta PC_1 = |PC_1^{(1)} - PC_1^{(2)}|$, and $\delta PC_2 = |PC_2^{(1)} - PC_2^{(2)}|$. The indexes (1) and (2) denote the two bodies in consideration. C_{PC} is a factor that weights the relative im-

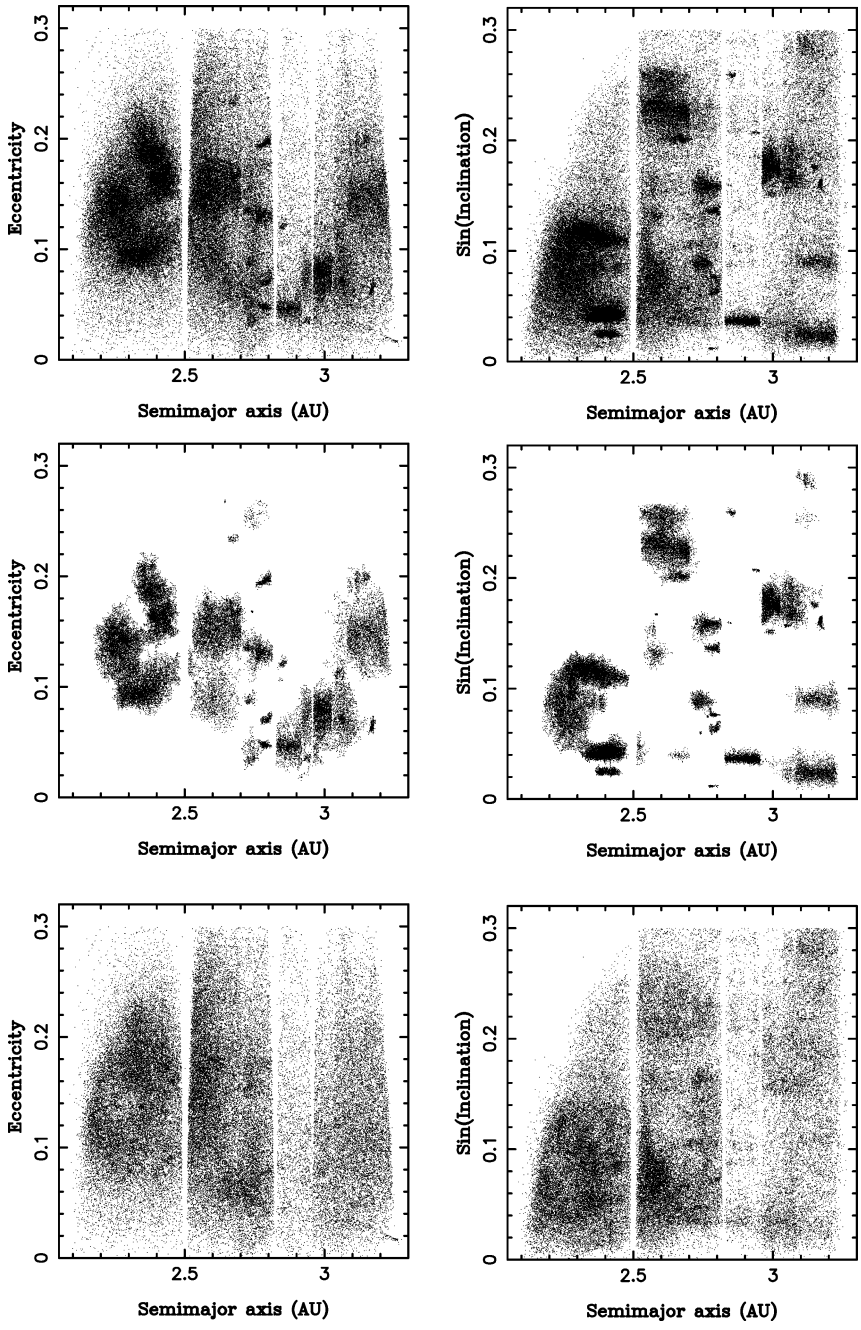

Fig. 6. Decomposition of the asteroid belt into family and background asteroids. From top to bottom, the panels show all main-belt asteroids, the family members, and the background asteroids, respectively.

portance of colors in our generalized HCM search. With d in m/s, we used typically $C_{\rm PC} = 10^6$ and varied this factor in the 10^4–10^8 range to test the dependence of results.

We have found no statistically robust concentrations in the extended proper element/color space that would help us to identify new families. This result shows that the list of families in Table 1 based on the available data is (at least nearly) complete. We have also found that the generalized HCM search is useful to identify family 'halos,' i.e., populations of peripheric family members that were not joined with the rest of the family with the standard HCM and cutoffs listed in Table 1. Some of these family halos may be also seen in bottom panels of Fig. 6 that show proper element distributions of the background asteroids (e.g., the Koronis family halo located at $a_{\rm P} = 2.9$ AU and small $i_{\rm P}$). Other halos, such as ~ 30 additional peripheric members of the Nysa–Polana (Cellino et al., 2001) family can be identified only in the extended proper element/color space, because they differ from their local background only by colors (i.e., $\mathrm{PC}_1 \lesssim 0$ for the Polana family).

By choosing cutoff distances d, we compromised (i) to include as many peripheric family members as possible, and

(ii) to avoid including many peripheric interlopers. The selected values of d that are listed in Table 1 are usually restrictive (i.e., at the small end of the acceptable range) because one of the goals of our study is to determine the reliable mean colors for family members. We thus tried to avoid including many peripheric interlopers by using small d.

In total, we have identified ~ 50 statistically robust asteroid families. We list 42 selected main-belt families in Table 1 (i.e., the Pallas family, other nonmain-belt families, and several substructures of the prominent main-belt families are not listed). Table 1 includes all most-reliable asteroid families listed in Bendjoya and Zappalà (2002); 25 in total, except a dispersed clump of asteroids around (110) Lydia (Zappalà et al., 1994, 1995), which the HCM failed to identify in the new proper elements catalog. The large overlap between our and previous family classifications shows the consistency of our approach. By using more proper element than previous studies, we found ~ 20 new, statistically-robust asteroid families.

4. Ages of asteroid families

Motivated by issues related to space weathering, we will examine the correlation between the SDSS colors of asteroids and their surface ages. Asteroid families are useful in this context because asteroid members of each family share the same origin (i.e., the same age). If we knew ages of asteroid families, we could better understand space weathering issues by studying color variations among them. For example, recent work has suggested that S-type asteroids with 'fresh' surfaces may have spectra that resemble (or trend toward) the ordinary chondrite spectra (see, e.g., Binzel et al., 2004, and references therein). If so, members of young S-type asteroid families (such as the Karin cluster; Nesvorný et al., 2002a) may show more OC-like colors than older S-type asteroid families (such as, e.g., the Koronis family; Marzari et al., 1995; Bottke et al., 2001).

To date, we know of four methods that allow us to estimate the age of an asteroid family: (i) Family Size-Frequency Distribution (SFD) Modeling, (ii) Global Main-Belt SFD Modeling, (iii) Modeling of Family Spreading via Thermal Forces, and (iv) Backward Numerical Integration of Orbits. We describe these methods below.

(i) *Family SFD modeling*. Marzari et al. (1995) have modeled the collisional evolution of three prominent asteroid families. Their collisional code evolves the initial SFD with time to match the modeled SFD with the observed SFD of a family. Using this method, Marzari et al. (1995) estimated that the Themis and Koronis families are of order 2 Gy old. These ages are uncertain because the initial SFD, scaling laws for impacts, and other parameters of the method are not known a priori. Moreover, in the case of the Eos family, Marzari et al.'s collision code generated no reasonable match to the observed SFD. Despite these limitations, Marzari et al.'s work was important because it showed that the prominent asteroid families are probably billions of years old.

(ii) *Global main-belt SFD modeling*. Durda and Dermott (1997) modeled the global collisional evolution of the main asteroid belt. Once the code is calibrated against the present SFD of the main belt, it can be used to calculate the typical time interval that elapses between breakups of diameter D asteroids. For example, Durda (personal communication) estimated that a $D \sim 100$-km asteroid disrupts somewhere in the main belt every 10^9 years, a $D \sim 50$-km asteroid disrupts every 2×10^7 years, and a $D \sim 30$-km asteroid disrupts every 5×10^6 years. Although these estimates have large uncertainties they show us that the large families that correspond to breakups of $D \sim 100$-km and larger parent bodies should be billions of years old, in agreement with (i). On the other hand, families originating from smaller parent bodies should be more numerous. For example, hundreds of asteroid families with $D \sim 30$ km parent bodies may have been produced in the asteroid belt since its formation. However, such a large number of small asteroid families is not observed today. One obvious solution to this problem is to invoke some erasure mechanism that eliminates small asteroid families over time. Indeed, a number of erasure mechanisms are operating in the asteroid belt today (Marzari et al., 1999; Bottke et al., 2001; Nesvorný et al., 2002b; Nesvorný and Bottke, 2004). It is thus likely that the observed asteroid families derived from smaller parent bodies are younger than those created by breakups of $D \gtrsim 100$-km parent bodies (such as the Themis, Koronis and Eos families).

(iii) *Modeling of family spreading via thermal forces*. A recent analysis has shown that the asteroid families are subject to slow spreading and dispersal via numerous tiny resonances in the main belt (Nesvorný et al., 2002b). Moreover, $D < 20$ km asteroids are moved inward toward the Sun and outward away from the Sun over comparatively long timescales by the Yarkovsky thermal effect; this mechanism provides another means for dispersing families (Bottke et al., 2001; Nesvorný et al., 2002b; Carruba et al., 2003; Nesvorný and Bottke, 2004). Therefore, old families' orbital parameters in (a_P, e_P, i_P) space do not reflect the immediate outcomes of cratering events or catastrophic disruptions. Instead, they reveal how the family members evolved in (a_P, e_P, i_P) space over long timescales by dynamical diffusion and chaotic resonances. On the other hand, tight clusters in (a_P, e_P, i_P) space should represent young families that have not yet had an opportunity to disperse via dynamical mechanisms. Using theoretical models of the Yarkovsky effect, D. Vokrouhlický (personal communication) estimated that the Eos family is 2.1 ± 0.5 Gy old, and Nesvorný et al. (2003) found that the Themis and Massalia families are 2.5 ± 1.0 Gy

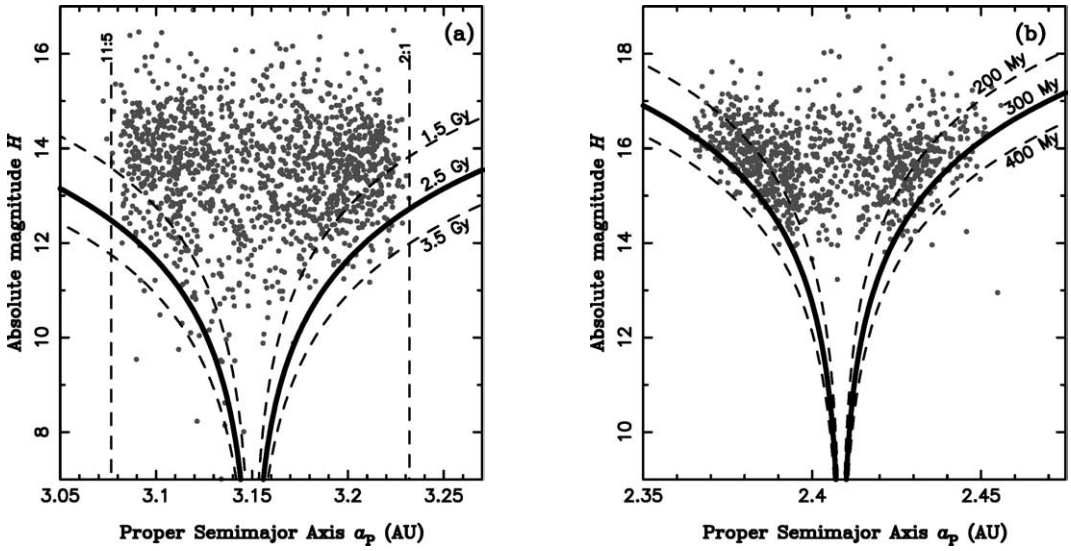

Fig. 7. Absolute magnitudes (H) and proper semimajor axes (a_P) of the Themis (a) and Massalia (b) family members (dots). The V-shaped lines indicate positions of Yarkovsky-drifting bodies evolved from the center of the families over the indicated time intervals, assuming maximum theoretical drift rates inward and outward. The drift rates were computed analytically using linearized approximations of the Yarkovsky effect (Vokrouhlický, 1999). Assuming a tight initial orbital distribution of a newly born family, the family members are expected to be localized within one of the V-shaped contours. In (a), the distribution in a_P of the Themis family members with $H \gtrsim 12.5$ is cut by the chaotic 11:5 and 2:1 mean motion resonances with Jupiter. Using members with $H \lesssim 12.5$, we estimate that the Themis family is 2.5 ± 1.0 Gy old. From (b), the Massalia family is 300 ± 100 My old. These estimates are robust over a wide range of the physical parameters compatible with the family's taxonomic type (Themis is C, Massalia is S) and with asteroidal surfaces covered by regolith. The outliers shown in the figure are probably interlopers. Figure from Nesvorný et al. (2003).

and 300 ± 100 My old, respectively. See Fig. 7 for a brief description of this method. Using the same method, W.F. Bottke (personal communication[12]) determined the approximate ages of many other asteroid families. We used the same means and determined ages for most asteroid families that we have identified.

When available, we list these ages in Table 1. These values are probably subject to a number of systematic and random errors. For example, physical parameters of asteroids such as the thermal conductivity, albedo, rotation speed, surface and bulk densities, etc., are generally unknown. The strength of the Yarkovsky effect depends on them in complicated ways (see, e.g., Vokrouhlický, 1999). On the other hand, recent studies (Chesley et al., 2003; Nesvorný and Bottke, 2004) used observations to directly detect the Yarkovsky effect and showed that the standard modeling of the Yarkovsky effect matches the observationally-measured semimajor axis evolution with reassuring precision. These results helped us to constrain some of the physical parameters that are most crucial for the correct modeling of the Yarkovsky effect (such as, e.g., the thermal conductivity). We estimate that the uncertainty in physical parameters produces up to $\sim 50\%$ uncertainties in the age estimates. These uncertainties cannot compromise our analysis (see next section) because the determined family ages range over three orders of magnitude.

A more fundamental limitation of an age estimate derived from the spread of an asteroid family in a_P is that some part of this spread may come from the collisional ejection of fragments rather than from the subsequent gradual spreading of the family members by thermal effects (Dell'Oro et al., 2004). This is probably not an important issue for most prominent families that are spread enough to allow us to gauge their age properly but poses difficulties for smaller and possibly younger families. For example, we know that the Karin cluster was generated by a breakup of a $\approx$ 30-km-diameter parent S-type body ≈ 5.8 My ago (Nesvorný et al., 2002a; Nesvorný and Bottke, 2004); this family is spread about 0.01 AU in a_P. Because the 1- to 5-km-diameter members of the Karin cluster drift at speeds of only about $3\text{–}5 \times 10^{-5}$ AU per My (Nesvorný and Bottke, 2004), the observed spread of the Karin cluster in a_P must have been generated by the breakup of the parent body rather than by the latter slow evolution; we estimate that it would take ~ 70 My for the Yarkovsky effect to generate the observed spread which is much longer than the actual family's age (≈ 5.8 My; Nesvorný et al., 2002a). To roughly compensate for the ejection field component, we assumed ejection speeds 'at infinity' $V_\infty \sim 15$ and $V_\infty \sim 30$ m/s for the S- and C-complex families, respectively. Ejection speeds of this order are suggested by dynamical structures of young asteroid families (Nesvorný et al., 2002a, 2003) and by the Smooth-Particle Hydrodynamics modeling of asteroid breakups (Michel et al., 2002, 2003). The difference between

[12] http://www.boulder.swri.edu~bottke/Yarkovsky/.

the assumed ejection speeds for S- and C-type families is related to different compositions of their parent bodies. For example, to explain structures of two known pristine asteroid families, the S-type Karin cluster and the C-type Veritas family, we find $V_\infty \sim 15$ and $V_\infty \sim 30$ m/s, respectively. These corrections produce ages that are about 70 and 140 My shorter than those determined if $V_\infty = 0$ is assumed.

We used the above corrections in an attempt to resolve an apparent problem with ages determined from $V_\infty = 0$: three families for which the rigorous method (iv) worked (see below) are all younger than 10 My (the Karin, Veritas and Iannini families). On the other hand, none of the ages determined from families' dispersions in a_P using $V_\infty = 0$ was larger than 10 My but shorter than 100 My even though we find no reason to believe that such ages should not occur. Although our solution of this problem may be simplistic, we adopted it to improve the consistency between methods (iii) and (iv).

Perhaps a more appropriate choice than a fixed V_∞ for all S- and C-type families would be to assume the initial spread of a family that increases (on average) with the size of the family's parent body (i.e., family-forming impacts in large bodies must produce larger ejection speeds so that fragments can escape). For example, Dell'Oro et al. (2004) argued that $\sim 50\%$ of the present spreads in the semimajor axis of prominent asteroid families is due to V_∞. If so, the age values determined with $V_\infty = 0$ should be reduced by a factor of ~ 2. We are developing a method where V_∞ and age can be fitted simultaneously to orbital distributions of at least several prominent families (Vokrouhlický et al., in preparation). This superior method will help us to obtain better understanding of V_∞ for family age estimates from (iii). Our preliminary results suggest values of V_∞ that are intermediate between the values assumed here and V_∞ recommended by Dell'Oro et al. (2004).

(iv) *Backward numerical integration of orbits*. To determine the exact age of a family the orbits of the family members must be numerically integrated into the past. The goal is to show that in some previous epoch the orbits of all cluster members were nearly the same (Nesvorný et al., 2002a). There are two angles that determine the orientation of an orbit in space: the longitude of the ascending node (Ω) and the argument of perihelion (ω). Due to planetary perturbations these angles evolve with different but nearly constant speeds for individual asteroid orbits. Today, the orbits of the family members are oriented differently in space because their slightly dissimilar periods of Ω and ω produce slow differential rotation of their orbits with respect to each other. Eventually, this effect allows Ω and ω to obtain nearly uniform distributions in $[0°, 360°]$. For a short time after the parent body breakup, however, the orientations of the fragments' orbits must have been nearly the same. Nesvorný et al. (2002a, 2003) used this method to determine the ages of the Karin (5.8 ± 0.2 My) and Veritas (8.3 ± 0.5 My) families, and also found that the tight family associated with (4652) Iannini is probably $\lesssim 5$ My old. Unfortunately, Nesvorný et al.'s method can not be used to determine ages of asteroid families that are much older than ≈ 10 My, because the orbital evolution of asteroids is usually chaotic and non-reversible on $\gtrsim 10$-My time scales.

In Table 1, we list ages for those asteroid families for which the age estimates are available. Ages of the Themis and Koronis families determined from (i) (~ 2 Gy) are consistent with determinations obtained from (ii) (~ 2.5 Gy). We list the latter values in Table 1, because we believe that (iii) generally provides a more reliable estimate of age. Similarly, (iv) is obviously more reliable and precise than (iii) for the young asteroid families.

We do not list age estimates for fourteen families in Table 1. In these cases, methods (i), (ii), (iii), and (iv) were found to provide unsatisfactory constraints on age or the age determination was not required because the spectral type of a family is clearly not C or S (families (3) Vesta and (1400) Tirela) and/or reliable mean values of PC_1 and PC_2 cannot be determined with the available data (families (283) Emma, (396) Aeolia, (1639) Bower, (9506) Telramund and (18405) FY12). For example, method (iv) does not work for any of these families because they are $\gtrsim 50$ My old and/or their recent orbital histories cannot be reproduced because of chaos. Method (iii) does not work for these families for a number of reasons. We list these reasons in the following paragraph.

(3) Juno and (4) Vesta families correspond to cratering events for which the contribution of ejection speeds to the present spreads of families in a_P may be large (Asphaug, 1997). Method (iii) fails in these cases because we cannot neglect this contribution and have no means to separate it from the subsequent spreading by thermal effects. (44) Nysa–Polana clan is a case of two families that overlap in a_P, e_P, i_P space and are difficult to separate (e.g., Cellino et al., 2002). (87) Sylvia family is located in a dynamically complicated region at $a_P \sim 3.5$ AU where chaotic resonances (rather than thermal effects) determine the dynamical structure of a family. Similarly, (46) Hestia and (2980) Cameron families (both S-type) were affected by strong chaotic resonances in the past (e.g., the 3:1 mean motion resonance for the Hestia family) that removed large fractions of their original populations. The dynamical structures of these families in a_P–H space (see Fig. 7) cannot be fit by a V-shaped boundary. (18405) FY12 family has only eleven known members. For this reason, its age cannot be reliably determined by method (iii) which is statistical in nature. Finally, (137) Meliboea family is a C-type family in the outer main belt that is probably >100 My old because of its large spread in a_P, e_P, i_P. The large fraction of dynamical interlopers ($\sim 30\%$ based on the SDSS colors) and the dif-

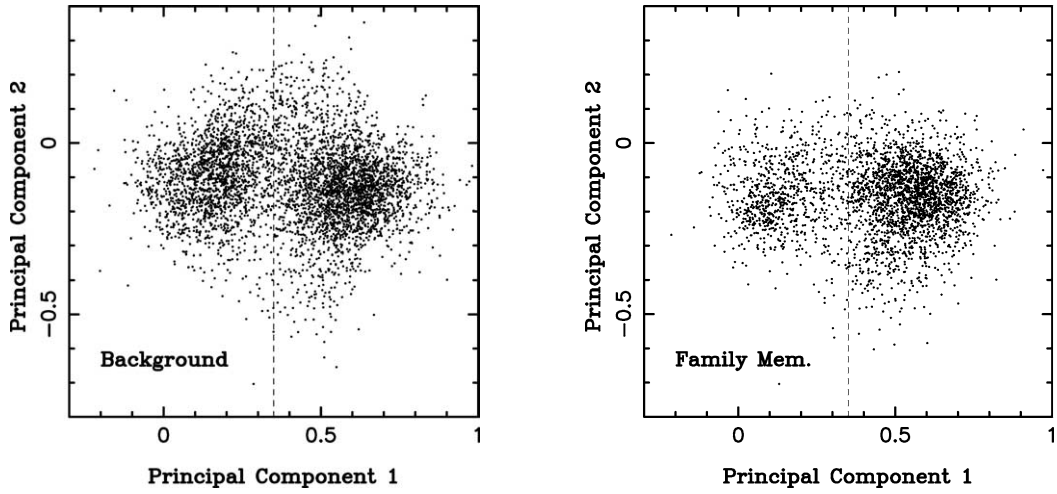

Fig. 8. Principal color components PC_1 and PC_2 of the main-belt asteroids observed by the SDSS. We show only those data points that have $\delta PC_1 < 0.1$ and $\delta PC_2 < 0.1$. From the total of 7593 main-belt asteroids, 3026 are family members (right panel), and 4567 are background main-belt objects (left panel). Vertical dashed line shows an approximate boundary between areas populated by the S- and C-complex asteroids. We study the color variations within these categories separately for family members.

ficulty to choose an adequate $d_{\rm cutoff}$ prevents us from better estimating the age of this family.

5. Colors of asteroid families

We used the subset of entries in the SDSS MOC that were matched to asteroids with known orbit elements (Jurić et al., 2002) and that have $\delta PC_1 < 0.1$ and $\delta PC_2 < 0.1$, where δPC_1 and δPC_2 are the measurement errors in the principal components.[13] In total, we studied colors of 7593 main-belt asteroids of which 3026 are family members and 4567 are background main belt objects (Fig. 8). In the following analysis we will concentrate on color variation between asteroid families and its correlation with their age. Other issues, such as the color variations within families, colors of the background population, etc., will be discussed elsewhere (Jedicke et al., in preparation).

Table 1 shows the taxonomic-complex types for families for which the classification was obvious according to our criteria defined in Section 2. In cases where the taxonomic type of a family was known previously from observations of its large members (see Cellino et al. (2002) and references therein) we find that this taxonomic type is also predominant for small asteroid family members observed by the SDSS (see also Ivezić et al., 2002). Our simple criteria, however, do not distinguish between subcategories within the three broad taxonomic complexes S, C, and X. For this reason, we list some families as being taxonomic S-complex type (i.e., part of the S-complex as defined by Bus and Binzel, 2002b) although a more refined classification is possible from the SDSS colors in some cases and/or the exact family's taxonomic type was determined by past spectroscopic surveys (see, e.g., Bus (1999) and Cellino et al. (2002)). Five families that appear to be either C- or X-complex type (no. 293, 363, 410, 1726 and 3556) are listed as C/X. For example, the (1726) Hoffmeister family is either C or F type according to Cellino et al. (2002).

Our Table 1 includes 24 families that were not listed in Cellino et al. (2002) because their taxonomic type was not known previously. On the other hand, Cellino et al. (2002) listed 11 families that are not included in our Table 1. Four of these families (14 Bellona, 88 Thisbe, 226 Weringia, 729 Watsonia) are very dispersed asteroid groups in proper element space and have been identified by means of spectroscopy rather than by the analysis of the proper elements. The (2) Pallas family is not included in our list because (2) Pallas has highly inclined orbit and does not appear in the catalog of analytically calculated proper elements that we use here. Three of Cellino et al.'s families (125 Liberatrix, 237 Coelestina, 322 Phaeo) were identified by means of the wavelet analysis of the proper elements. These families are statistically less robust because the wavelet analysis is known to impose more relaxed criteria on family membership than the HCM (Zappalà et al., 1995). The (2085) Henan and (110) Lydia families are rather dispersed, possibly old families that we have failed to identify as reliable asteroid families by using the most recent proper element catalog. Finally, the HCM fails to identify Cellino et al.'s (45) Eugenia family with $d \leqslant 120$ m/s, while all our other families show many members with $d \leqslant 120$ m/s values. Given the goals of this study we favor more restrictive criteria for family membership and will not use these families in our analysis.

We selected those families that are clearly either S-, C-, or X-complex type. Unusual cases, such as the Flora and Erigone families that show many members with SDSS colors corresponding to two or more distinct taxonomic complexes, were excluded from the analysis. Next, we removed

[13] For those asteroids that were observed more than once by the SDSS, we use the color measurement that has the smallest error.

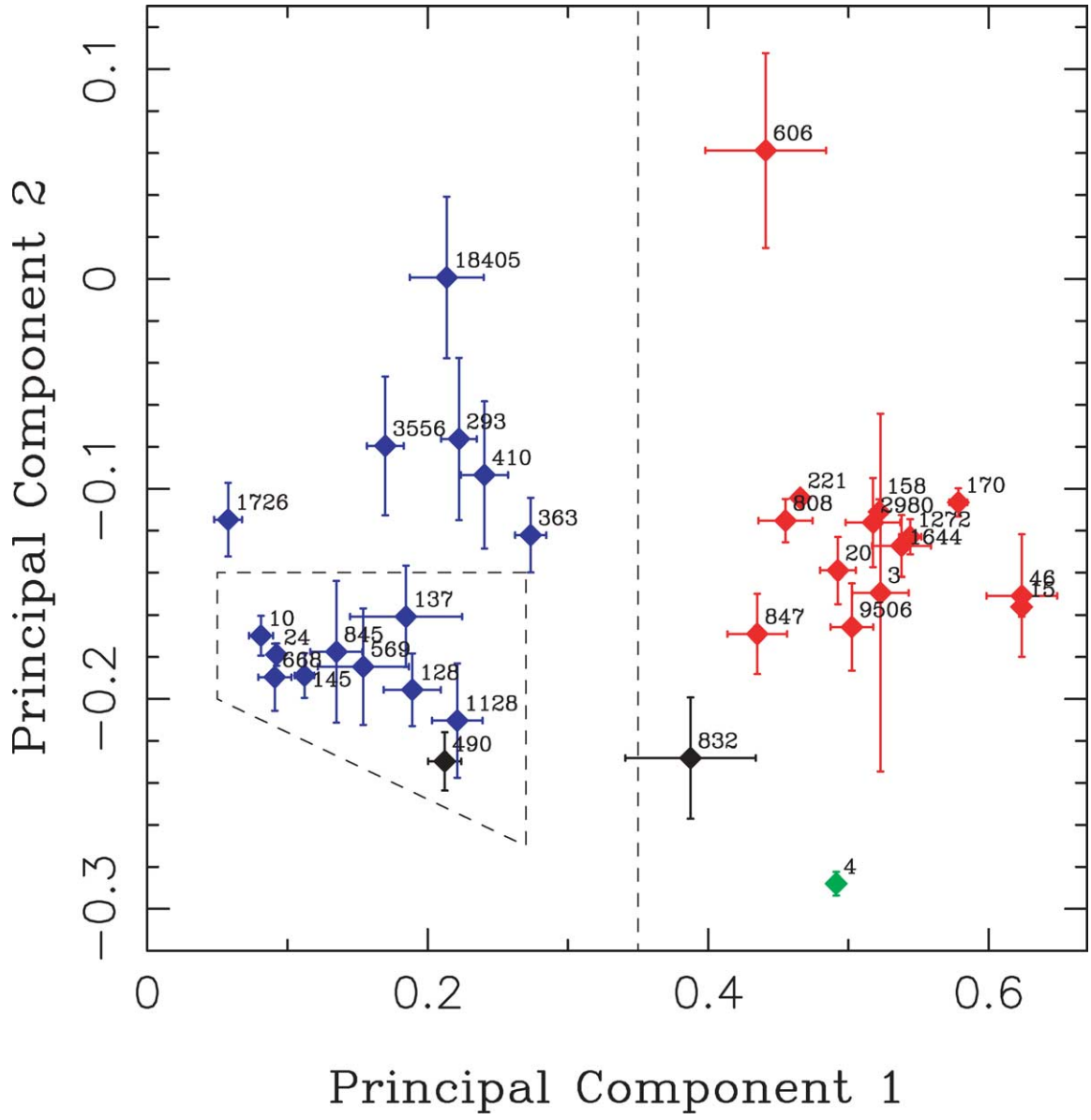

Fig. 9. Principal color components PC_1 and PC_2 for asteroid families. As shown in Fig. 10 and discussed in the related text, PC_1 is a proxy for the spectral slope and PC_2 is related to the spectral curvature. The bars show 1σ errors of mean PC_1 and PC_2 calculated over all family members with $\delta PC_1 < 0.1$ and $\delta PC_2 < 0.1$. Only families with at least two members matching this criterion are shown. We also do not show families with ambiguous taxonomic types such as the Flora and Erigone families (see Table 1). The C- (blue) and S-complex (red) families clearly segregate in PC_1 by the vertical dashed line at $PC_1 = 0.35$. The dashed polygon delimits the group of C-complex families that have similar colors. Six C- and X-complex families appear outside the limit of this region, have larger PC_2, and span large color range. The recently-formed (490) Veritas and (832) Karin families are denoted in black. Their colors are located at a periphery of well defined regions in (PC_1, PC_2) plane that are populated by the "blue" and "red" families, respectively. Note the large color difference between the (832) Karin and (158) Koronis families. The Vesta family (green) has the smallest mean PC_2 value among the identified families; the (606) Brangane family has the largest mean PC_2 value.

all interlopers from the S-, C-, and X-complex families (e.g., those member asteroids that have unusual colors relative to the most other members), and calculated $\langle PC_1 \rangle$ and $\langle PC_2 \rangle$, where $\langle PC_j \rangle$ is the arithmetic mean of the jth principal component over the remaining members of each asteroid family.

Figure 9 shows the mean colors of S-, C- and X-complex families. The S-complex families have $PC_1 > 0.35$ while C- and X-complex families have $PC_1 < 0.35$. The V-type Vesta family (denoted in green) differs from the S-type families by small PC_2. The (832) Karin cluster and the (490) Veritas family, the two youngest known asteroid families for which we have good color data, are located on a periphery of regions in (PC_1, PC_2) plane that are populated by the S- and C-type families. There is a significant spread of PC_1 and PC_2 for families of the same taxonomic complex. For example, two C-complex families can differ by ~ 0.1–0.2 in PC_1 and/or PC_2. Because measurement errors and errors of the mean colors are $\lesssim 0.05$, Fig. 9 documents true color differ-

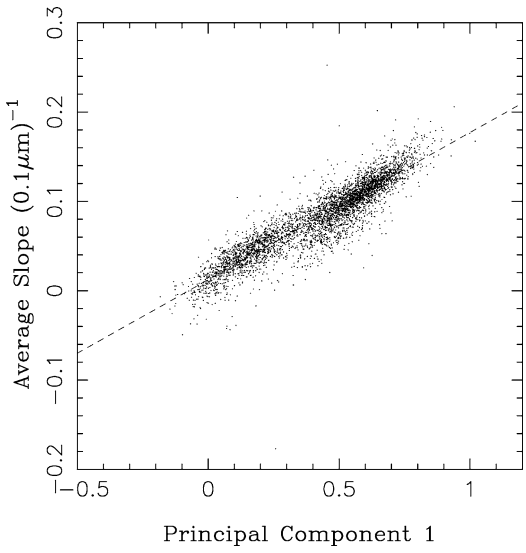

Fig. 10. Relation between PC_1 and the average spectral slope measured between 0.35 and 0.9 μm. The average slopes have been calculated from five colors listed in the SDSS MOC for those measurements that have $\delta PC_1 < 0.1$ and $\delta PC_2 < 0.1$. PC_1 is a strong function of the spectral slope. The dashed line is the best linear fit with average slope $\propto 0.165 \times PC_1$.

ences between families. This result is consistent with studies of spectral variability among families by higher-resolution spectrophotometric measurements (cf. Cellino et al., 2002).

A simple explanation for this behavior is to interpret colors in terms of mineralogical differences between parent bodies of asteroid families. To this end, we must know how PC_1 and PC_2 correlate with spectral features that are diagnostic for presence of specific minerals. Figure 10 shows that PC_1 is an effective measure of the average spectral slope between 0.35 and 0.9 μm. On the other hand, PC_2 correlates with the spectral curvature generated by broad absorption features such as the 1-μm olivine/pyroxene absorption band (e.g., Gaffey et al., 2002). These spectral features are also affected by asteroid surface properties such as the presence of particulate regolith, temperature, etc. (e.g., Johnson and Fanale, 1973; Roush and Singer, 1984). Moreover, the spectral slope and the depth of the 1-μm absorption band is affected by space weathering processes (e.g., Pieters et al., 2000; Hapke, 2001; Clark et al., 2002a; Chapman, 2004).

To address these issues, we searched for correlations of PC_1 and PC_2 with asteroid size, distance from the Sun, age of an asteroid family, etc. Interestingly, the only statistically significant correlation we found is a correlation between PC_1 and the age of an asteroid family. Figure 11 shows a plot of PC_1 as a function of age for selected S- and C-complex asteroid families: (a) all S-complex families that appear in Fig. 9 but (606) Brangane; we also include the S-type (4652) Iannini family in Fig. 11 using its members with $\delta PC_1 < 0.3$ and $\delta PC_2 < 0.3$.[14] (b) All C-complex families that appear in a dashed polygon in Fig. 9. We plot only these C-complex families in Fig. 11 because we have found that the remaining six C- and X-type families do not show a clear correlation between PC_1 and age. We motivate this selection by the fact that families such as, e.g., the (18405) FY12 family with mean $PC_2 \sim 0$, are likely to have a very different mineralogical composition from the C-complex families. For the same reason we exclude the (606) Brangane family from the analysis of the S-complex families because it has unusually large PC_2 (cf. Jedicke et al., 2004).

The trends for S- and C-complex families in Fig. 11 are opposite. Young S-complex families generally have smaller PC_1 than old S-complex families, while young C-complex families tend to have larger PC_1 than old C-type families. This produces a sort of convergence, where in the limit of zero age the S- and C-complex families would converge have similar values (~ 0.3) of PC_1. This does not mean that spectra of the S- and C-complex families become identical in the limit of zero age; they differ in dimensions orthogonal to PC_1.

We assign these color vs. age trends to effects of space weathering. In our scenario, surfaces of the member asteroids of a family were initially covered by a (perhaps thin) layer of 'fresh' particulate material that had been excavated by the disruption event from the parent body interior. This is consistent with recent results that favor low values of the surface thermal conductivity for Karin family members (Nesvorný and Bottke, 2004). This surface material was then subject to space weathering effects. Spectral changes produced by these effects over time should be similar for all member asteroids of a single asteroid family, because they should have similar mineralogy (Bus, 1999) and their surfaces have the same age. Because PC_1 is a proxy for the spectral slope (Fig. 10), Fig. 11 suggests that colors of S- and C-complex asteroids become increasingly 'red' and 'blue' over time, respectively. The former result confirms findings of Jedicke et al. (2004) and is consistent with previous studies of space weathering by remote sensing and ground-based spectrophotometry (see Clark et al., 2002a; Chapman, 2004, for reviews).

Figure 11 shows that there is an age-dependent component to asteroid colors along with mineralogical differences. Because we have no a priori means of disentangling these effects we make no distinction between families of different taxonomic types within the S- and C-complexes. Some justification for this approach is suggested by the large color difference between the (832) Karin and (158) Koronis families. The Karin family was formed by a breakup of a former Koronis family member (Nesvorný et al., 2002a). For

[14] It may be debatable whether or not the Iannini family should be included in the current analysis because we do not have good SDSS color data for this family (i.e., none of its members has $\delta PC_1 < 0.1$ and $\delta PC_2 < 0.1$). Moreover, the spectral classification of this family is uncertain because of its unusual PC_2 value (Table 1; it is likely an S-complex family because it is located in the inner part of the main belt that is predominantly populated by S-type objects). For these reasons, our interpretation of the SDSS colors for this family should be taken with caution.

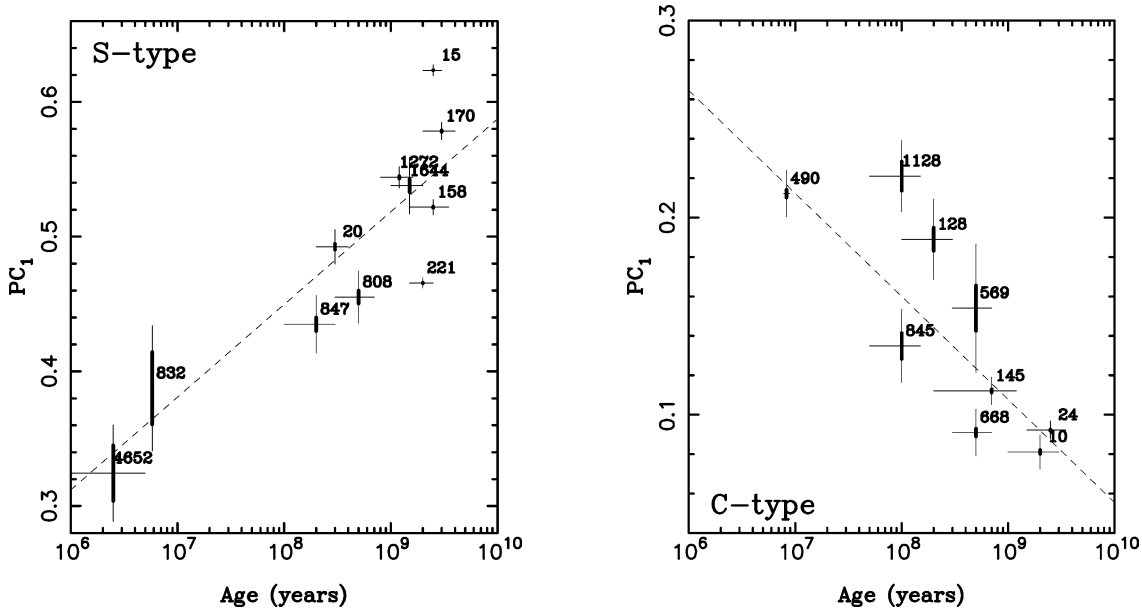

Fig. 11. Principal color component PC_1 as a function of age for the S- (left panel; adapted from Jedicke et al., 2004) and C-complex asteroid families (right panel). We plot here only those C-complex families that appear in the polygon area in Fig. 9. Each family is denoted by its lowest numbered member asteroid. For example, 832 and 158 in the left panel denote the Karin and Koronis families, respectively; 490 and 24 in the right panel denote the Veritas and Themis families, respectively. The horizontal bars show errors of family age estimates. The thin vertical bars show RMS variations of PC_1 within each family and represent true color variations among family members. The standard errors of mean PC_1 are denoted by shorter, bold vertical bars. Both S- and C-complex families show correlations between PC_1 and age. These correlations (denoted by dashed lines) are statistically significant. The trends are opposite. Young S-complex families generally have smaller PC_1 than old S-complex families, while young C-complex families tend to have larger PC_1 than old C-complex families. The dashed lines show our best log-linear fits to these trends.

this reason, the Karin and Koronis family asteroids should be compositionally similar. Yet, their SDSS colors differ (Fig. 9). It is natural to assign this color differences to space weathering effects because the Karin family is one of the most recently-formed families in the asteroid belt (5.8 ± 0.2 My old (Nesvorný et al., 2002a)) while the Koronis family is one of the oldest ($\sim$ 2–3 Gy old; Marzari et al., 1995; Bottke et al., 2001).

The trends in Fig. 11 cannot be explained by assuming that the mean SDSS color varies with asteroid size rather than with family age. On one hand it is true that younger families have usually smaller parent bodies, because small main-belt asteroids are disrupted at higher rates than large ones. Also, fragments of small parent bodies are smaller than those produced by breakups of large parent bodies. On the other hand, the mean SDSS colors are dominated by small, $H \gtrsim 13.0$ asteroids which are abundant in both the large and small families. For this reason, the correlation between the SDSS's PC_1 and age occurs independently of whether we do or do not consider a size-limited sample of family members. We have made this and other tests and found no correlation of color with size. We also argue that the parent body of the young Veritas family ($\sim$ 140 km in size; Tanga et al., 1999) was larger than parent bodies of many prominent old families. Thus, the colors of the Veritas family (Fig. 9) may bear signatures of the recent origin of this family rather than being determined by the size of its parent body.

Correlations between PC_1 and $\log_{10} t$ have been fit by straight lines. We used the `fitexy` routine from Numerical Recipes (Press et al., 1992) which let us fit PC_1 vs. $\log_{10} t$ accounting for errors associated with both values (for PC_1 errors, we used the RMS range of PC_1 values within the family). The dashed lines in Fig. 11 show our best-fit results. For the S-complex families, we found that $PC_1 = A \log_{10} t + B$ (t in My) with $A = 0.068 \pm 0.024$ and $B = 0.312 \pm 0.060$, where the formal errors were determined by `fitexy`. The real uncertainty of this empirical fit must be larger than the formal errors because of the effect of varying composition among the S-complex families. The slope of the distribution is significant at greater than the 3σ level and there is a 76% correlation coefficient between PC_1 and $\log_{10}(t)$. For the C-type families, we found a less robust correlation with the best-fit parameters given by $A = -0.052 \pm 0.023$ and $B = 0.265 \pm 0.076$.

Using Fig. 10 that relates PC_1 with the spectral slope, we find that the mean spectral slope of the S-complex families increases with time as $\approx 0.01\ \mu m^{-1} \times \log_{10} t$. This empirical fit is valid only for $2.5 \lesssim t \lesssim 3000$ My (the time interval where we have data) and for the mean spectral slope determined from wide-wavelength filter photometry obtained by the Sloan Digital Sky Survey (for reasons discussed in Section 2). This result is as one would intuitively expect—the rate of space weathering is greatest for freshly exposed surfaces and as the object ages there is less opportunity for more weathering to occur on an already weathered surface. The functional form of the fit that we use here is arbitrary. We choose it because the log-linear fit is simple and does not require any special assumptions about the nature of space

weathering effects. See Jedicke et al. (2004) for an alternative, theoretically-motivated form of the fit function. See Pieters et al. (2000) and Noble et al. (2004) for a discussion of factors that determine the space weathering rate as a function of time.

The correlation shown in Fig. 11 for the S-complex families would be much weaker than calculated above if the data points corresponding to the youngest families (such as the Iannini, Karin and Agnia families) were excluded from the analysis. For this reason, the youngest families provide a crucial constraint on our scenario. Fortunately, the youngest of all, the Karin and Iannini clusters, are robust dynamical families with solid age determinations (Nesvorný et al., 2002a, 2003; Nesvorný and Bottke, 2004). Also, the S-complex members of the Iannini cluster have distinct colors from their local background of predominantly C-type asteroids. It is thus difficult to explain the colors of Karin and Iannini cluster members by using other assumptions.

The young Veritas family and the old Themis and Hygiea families are similarly important to constrain the color-age correlation for the C-complex families in Fig. 11. The Veritas family is a robust dynamical family with solid age determination (Milani and Farinella, 1994; Nesvorný et al., 2003). The ages of the Themis and Hygiea families are certain only to about $\sim 50\%$. Figure 11 shows asteroid family ages over a three orders of magnitude range: the Iannini, Karin, and Veritas families being the youngest (< 10 My) and the Maria family being probably the oldest (~ 3 Gy). For this reason, $\sim 50\%$ errors in some family age estimates cannot compromise our results.

As was argued earlier, some part of the PC_1 variability between families must come from the compositional variability between their parent bodies. For this reason, the spread of data points around the best-fit lines in Fig. 11 is not surprising. On the other hand, we find it hard to believe that compositional variability has a dominant effect in Fig. 11, because we do not see any reason why colors of young families would differ from colors of old ones.

To probe the effect of composition we compared the reflectance spectra of the S-complex Karin and Koronis families (Fig. 12). Because the Karin cluster was produced by a breakup of a former Koronis family member, the mineralogical composition of these families should be similar. In contrast, the spectral slopes at 0.5–0.9 μm of Karin cluster members are significantly shallower than the spectral slopes of Koronis family members (Fig. 12). Moreover, the Karin cluster members show an absorption feature at ~ 0.9 μm that is deeper than that of Koronis family members. We find about 15% difference in flux at ~ 0.9 μm when the flux is normalized at ~ 0.55 μm. This comparison shows that the difference in composition among the S-complex families cannot account for the color trends of S-complex families in Fig. 11.

Unfortunately, a similar comparison can not yet be made for the C-complex families because we have not yet identified a recent breakup of a member of an old C-complex family. We may, however, compare the colors of the Veritas family (youngest known C-complex family) with some compositional analog. Possible analogs are the Themis and Hygiea families. These families are located in the same region of the main belt as the Veritas family ($a \sim 3.2$ AU) suggesting that their parent bodies may have accreted from roughly the same part of the proto-planetary disk. The Themis and Hygiea families are also the oldest C-complex families known (2.5 ± 1 and 2 ± 1 Gy, respectively; Table 1). By comparing their colors with the 8.3 ± 0.5 My old Veritas family, the effects of space weathering can be best identified. Because the Themis and Hygiea families have nearly identical colors, we concentrate on the comparison between the Veritas and Themis families (Fig. 13).

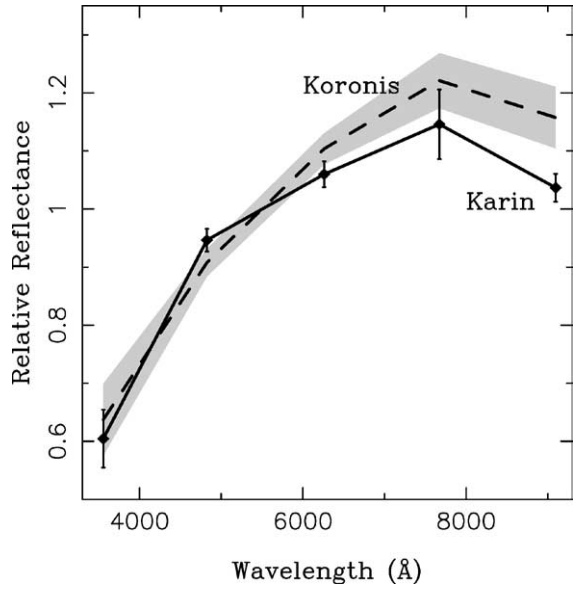

Fig. 12. SDSS spectrophotometric data for the S-complex Koronis and Karin families. Using the same method as in Fig. 2, we plot the mean reflectance of Koronis family members that have $\delta PC_1 < 0.1$ and $\delta PC_2 < 0.1$ (dashed line), and the RMS variation of the reflectance within the Koronis family (shaded area around the dashed line). The mean spectral reflectances for the Karin cluster (solid line with RMS bars at effective wavelengths of the SDSS filters) were calculated with the same criteria. The Karin cluster shows a shallower spectral slope and deeper 1-μm absorption band than the Koronis family.

Figure 13 illustrates the spectral difference between the two families. The spectral slope of the Veritas family is on average steeper than that of the Themis family. No counterpart exists among the Themis family members for the steep spectral slope at short wavelengths that is typical for the Veritas family members. Other young C-complex families (such as, e.g., the (1128) Astrid family) have spectral slopes that are similar to that of the Veritas family. We believe that these facts may indicate that the space weathering processes modify colors of the C-complex asteroids over time. We cannot exclude that compositional differences between the C-complex families cause these spectral variations. If the Veritas, Themis and Hygiea families are removed from Fig. 11, evidence for the age–color correlation among the C-complex families becomes statistically insignificant.

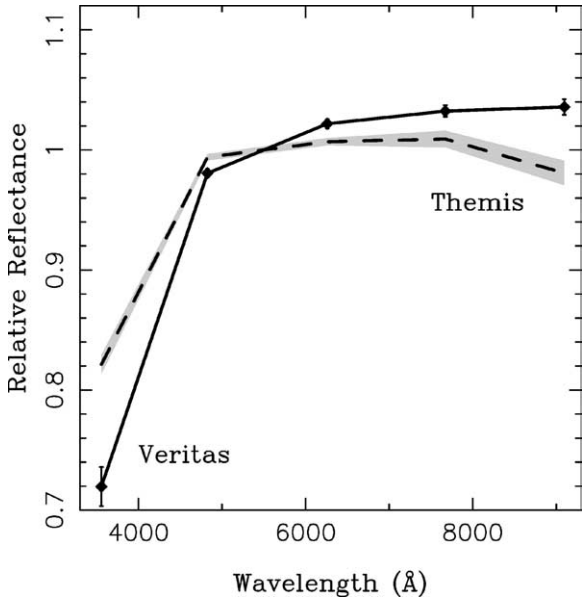

Fig. 13. SDSS spectrophotometric data for the C-complex Themis and Veritas families. We plot the mean reflectance of Themis family members that have $\delta PC_1 < 0.1$ and $\delta PC_2 < 0.1$ (dashed line), and its standard error (shaded area around the dashed line). The mean spectral reflectances for the Veritas family (solid line with error bars) were calculated with the same criteria. The mean spectral slope of the Veritas family is steeper than the mean spectral slope of the Themis family.

6. Summary and discussion

Our work provides new evidence for space weathering effects. Using a novel method, we found that the reflectance spectra of the S-complex asteroids become redder and that the broad absorption band at 1 μm becomes shallower over time. We measured the rate of these spectral changes. We estimated that the mean spectral slope between 0.35 and 0.9 μm increases with time t (given in My) as $\approx 0.01\ \mu m^{-1} \times \log_{10} t$. This empirical fit is valid only for $2.5 \lesssim t \lesssim 3000$ My and cannot be easily extrapolated to arbitrarily small or large t. We also found that Gy-old terrains of S-type asteroids reflect about 15% more light at ∼1-μm wavelengths than an ∼5-My-old S-type asteroid surface when the flux is normalized by the reflected light at 0.55 μm. These spectral changes were determined from the wide-wavelength filter photometry obtained by the Sloan Digital Sky Survey. Because the SDSS filters integrate the spectral reflectance over their 0.1–0.3-μm widths (issue discussed in Section 2), caution is required to compare the determined spectral changes with other recent studies of space weathering effects that used higher-resolution spectra (e.g., Clark et al., 2001, 2002a, 2002b; Murchie et al., 2002; Chapman, 2004; Binzel et al., 2004).

The S-complex families with <10 My ages (832 Karin and 4652 Iannini) are important in establishing the age–color correlation for the S-complex families. The ages of these young families were determined by the most reliable method (iv) described in Section 4. On the other hand, 1σ errors of mean PC_1 and PC_2 for these families are among the largest among the S-complex families because only a small number of their dynamical members were observed by the SDSS. We expect this situation will improve when new, enlarged releases of the SDSS MOC will become available. Unfortunately, only one recent C-complex family is known (490 Veritas). This makes it more difficult to obtain conclusive evidence for the space weathering processes on the C-complex asteroids. Nevertheless, we found a correlation between ages and colors for the C-complex families. If real, this result suggests that the C-complex asteroids show spectral alterations by space weathering effects that decrease their mean spectral slope over time. This result needs verification. When a new young C-complex family is identified in the main belt we predict that its members will show spectral slopes similar to those of the Veritas family members.

The opposite trends in weathering effects for S- and C-complex asteroids could be due to the compositional differences between the two general types of asteroids. More experimental work needs to be done on space weathering of carbonaceous materials before this issue can be understood. The inherent opacity of carbonaceous material prevents transmission and multiple scattering, and suppresses both the spectral features and any process that may modify them (e.g., Shingareva et al., 2003). For example, experiments on vapor-deposited nanophase iron show this effect lessens for the low-albedo surface of carbonaceous chondrites. These results explain the lack of color and albedo variations on (253) Mathilde (Veverka et al., 1999; Clark et al., 1999). Another possibility is that the regolith surface of a hydrated asteroid could devolatilize and dehydrate over time. Indeed, there is a mixture of dry and hydrated objects among the low-albedo asteroids (Rivkin et al., 2003). In this scenario, the hydrated minerals which become exposed from the deep interior of the parent body by the family-forming impact loose their water content over time. It is not clear, however, whether (i) the hydrated minerals can retain their water content during the family-forming impact, and (ii) whether the optical properties of hydrated minerals are compatible with the SDSS colors of young C-type families (such as the (490) Veritas family; Fig. 13).

An intriguing application of the determined weathering rates is the possibility to estimate surface ages for individual S- and C-complex asteroids from their color. A systematic study of this problem, however, goes beyond the scope of the present study.

Our work has important implications for the origin of ordinary-chondrite (OC) meteorites which are the most abundant class of meteorites found on the Earth. The reflectance spectra of OC meteorites that are obtained in laboratories show a shallow spectral slope and very deep olivine/pyroxene absorption bands, which are uncommon spectral features among the main-belt asteroids. This is surprising because meteorites are fragments of the main-belt asteroids (e.g., McSween, 1999); the spectral characteristics of the OC meteorites and many main-belt asteroids should thus be similar.

To resolve this apparent paradox, Chapman and Salisbury (1973) proposed a number of processes that may account for the observed difference. More recently, color variations on surfaces of S-type asteroids observed by the Galileo and NEAR spacecrafts ((243) Ida, (951) Gaspra, (433) Eros) provided strong evidence for the space weathering hypothesis because older surface terrains were found to be darker and redder in appearance (Veverka et al., 2000; Clark et al., 2001, 2002a, 2002b; Murchie et al., 2002; Chapman, 2004) than some geologically recent surface markings. Micrometeorite impacts and/or solar wind irradiation that produces nanophase iron particles on asteroid regolith grains is thought to be responsible for these spectral alterations (Cassidy and Hapke, 1975; Hapke, 2001; Pieters et al., 2000; Sasaki et al., 2001).

Our results shows that there is an age-dependent component to asteroid colors along with mineralogical differences. We cannot disentangle these two effects because we do not distinguish between taxonomic subcategories of the C- and S-complexes. For example, Gaffey et al. (1993) proposed a classification scheme based on mineralogical absorption features in the near IR that suggests that only one subcategory of the S-complex, S(IV), is mineralogically similar to OC meteorites. Unfortunately, our analysis cannot be restricted to those families of the S(IV) type because: (1) the Gaffey et al.'s mineralogical classification scheme has only been applied to 39 asteroids, (2) that classification scheme ignored the possibility of space weathering, assigning all spectral variability withing the S-complex to mineralogical diversification, and (3) the limited wavelength range of the SDSS filters does not allow us to classify asteroids into the Gaffey et al.'s S-complex subcategories. Similarly, the (221) Eos family contains many K-type (taxonomic subcategory within the S-complex) asteroids that are thought to be related to the CO3 and CV3 chondrites rather than the OC meteorites (Doressoundiram et al., 1998).

By contrasting colors of the S-type Koronis and Karin families we found that compositional differences can not account (entirely) for the SDSS color differences. The Koronis family originated from a compositionally homogeneous (probably nondifferentiated) parent asteroid because its member asteroids show homogeneous colors. The Karin cluster formed as a result of breakup of a $\sim$30-km-diameter Koronis family member. The asteroids in the Karin cluster must be compositionally similar to the Koronis family members. Yet the colors differ (Fig. 9). It is also difficult to explain how compositional differences could produce the trends shown in Fig. 11.

Because we were able to measure the space weathering rate for S-complex asteroids we can draw several important conclusions for the origin of OC meteorites and for the surface geology of asteroids. According to our results, the reflectance spectrum of the S-complex asteroids with a few-million-year surface age (such as members of the Karin or Iannini families) appears to be converging toward that of OC meteorites. This result presents strong support for earlier speculations that many S-complex asteroids could be OC meteorite parent bodies.

The Azzurra impact crater, its ejecta, and some small, morphologically fresh craters imaged by the Galileo spacecraft at (243) Ida (a member of the Koronis family) show bluer-than-average colors and the 1-μm absorption band that is $\sim$ 10–15% deeper (flux normalized at $\sim$ 0.55 μm) than the same spectral band observed on Ida's weathered terrains (e.g., Veverka et al., 1996; Sullivan et al., 1996). Comparing these values with the ones found in our study (e.g., Fig. 12), we find that the youngest studied surface features on Ida have ages that are comparable to or somewhat older than that of the Karin cluster (i.e., $\gtrsim$ 6 My). This result has important implications for the geology of (243) Ida. In principle, the morphologically fresh craters on Ida could be given absolute dates by carefully sorting their spectra and by using the space weathering rate that we have determined.

The Near-Earth Objects (NEOs) show an abundance of so-called Q-type asteroids (about 20% of $\approx$ 300 surveyed NEOs are Q-types; see Binzel et al. (2002) for a recent review), which are direct spectrophotometric analogs for the ordinary chondritic material. In contrast, no Q-type asteroid has been found to date among the $\sim$ 2000 surveyed main belt asteroids (MBAs; e.g., Bus and Binzel, 2002a, 2002b). This lack of spectrophotometric main-belt analogs for the OC meteorites is a long-debated and fundamental problem. It is now generally accepted that space weathering processes similar to those acting on the Moon (Gold, 1955; Pieters et al., 2000; see Hapke, 2001, for a review) can darken and redden the initially OC-like (Q-type) spectrum of a fresh asteroid surface, giving it an S-type appearance (see Clark et al. (2001, 2002a, 2002b); and Chapman (2004) for direct evidence for space weathering processes from the NEAR-Shoemaker and Galileo spacecrafts, and Bus and Binzel (2002b) for a definition of Q-type spectra).

The canonical interpretation of these results is that the lack of Q-type asteroids among the observationally sampled MBAs is related to asteroid-size-dependent effects on surface regolith or to the shorter collisional lifetimes of smaller asteroids (e.g., Johnson and Fanale, 1973; Binzel et al., 1998, 2001, 2002, 2004; Rabinowitz, 1998; Whiteley, 2001). Indeed, current spectrophotometric surveys of MBAs are largely incomplete in the size range of typical NEOs ($\lesssim$ 5-km diameters).

Researchers hypothesize that: (i) Survival lifetimes against catastrophic disruption (see Davis et al., 2002) decrease with decreasing size. Thus, on average, as we examine smaller and smaller objects, we should see younger and younger surfaces. (ii) Surfaces showing Q-type spectral properties should thus exist, on average, only among the smallest asteroids, which become easy spectroscopic targets only when they enter into NEO space. (iii) Large, OC-like asteroids in the main belt should show, on average, 'space-weathered' spectral properties, explaining why they are taxonomically classified as S-type asteroids.

There are several problems with this "standard scenario." For example, many km-sized and larger Q-type NEOs can be found that have collisional lifetimes $\gtrsim 100$ My (a recent study by Bottke et al. (2002) suggests their $\gg 100$ My collisional lifetimes). Yet, our measurements of the space weathering rate (see also Jedicke et al., 2004; Yoshida et al., 2004; Sasaki et al., 2004) suggest that space weathering processes operate on shorter timescales ($\lesssim 10$ My) to modify the Q-type spectrum into the S-type spectrum (i.e., produce a steeper spectral slope, suppress 1- and 2-μm absorption bands; e.g., Hapke, 2001). If so, we require that the observed Q-type NEOs have surface ages that are $\lesssim 10$ My. This implication of the standard scenario is at odds with the collisional and dynamical models of the NEOs' origin because it requires that $\gtrsim 20\%$ of NEOs were produced by collisional breakups of large bodies within the past $\lesssim 10$ My. In contrast, models predict much longer durations for processes like the Yarkovsky effect and small resonances to insert collisional fragments into the planet-crossing space (e.g., Migliorini et al., 1998; Bottke et al., 2002; Morbidelli and Vokrouhlický, 2003; Binzel et al., 2004). Whiteley (2001) and Binzel et al. (2002) discuss other objections to the standard scenario.

To resolve these problems, we propose a new scenario for the origin of Q-type NEOs that assumes that surfaces of Q-type NEOs have been recently (i.e., within the past $\lesssim 10$ My) reset by tidal effects. To show that this scenario is plausible, we estimate that a typical NEO suffers on average about one encounter to within 2 Roche radii ($R_{\rm Roche}$) from the Earth every ≈ 10 My. This time interval between encounters is comparable with the average orbital lifetime of NEOs (≈ 5 My according to Bottke et al., 2002) and is also comparable with the range of space weathering timescales that we determine here. Consequently, if tidal encounters at $2R_{\rm Roche}$ can reset the surface, Q-type NEOs could be as numerous as S-type NEOs. Perhaps only closer encounters matter. For comparison, encounters up to five planet radii (this limit depends on shape and spin rate) can produce strong distortions of a rubble-pile NEO and material stripping that accounts up to 10% of the preencounter NEO's mass (Richardson et al., 1998). If our scenario is correct, Q-type asteroids must be rare among the MBAs.

The SDSS MOV is the only resource available to us that shows a correlation of spectrum with age for the asteroid families. Conversely, we were not able to identify any significant change as a function of time for asteroid albedo values listed in the Supplementary IRAS Minor Planet Survey (SIMPS, Tedesco et al., 2002) and for the J/H and K/H near-IR band ratios listed in the 2-Micron All Sky Survey (2MASS, Sykes et al., 2000). This might be due to a lack of sensitivity of our technique (e.g., space weathering occurring too fast) and could indicate that different processes act at varying time scales to create the overall space weathering phenomenon. For example, Pieters et al. (2000) and Noble et al. (2004) found that small degrees of space weathering more strongly influence the visible region of spectra, while leaving the near-IR largely unaffected.

The 5-color photometry obtained by the Sloan Digital Sky Survey is the only current source that provides spectral information for small asteroid families. For example, none of the Karin and Iannini cluster members have been observed by SMASS (Bus and Binzel, 2002a). Spectra of these families are essential to determine the rate of space weathering on My time scales. To verify our results it is thus crucial to obtain good visible and near infra-red spectroscopic data on a representative number of members of the Karin and Iannini families, as well as of any other recently-formed families that may be discovered in the future.

Acknowledgments

We thank Bill Bottke, Beth Clark, Clark Chapman, and Jeff Taylor for their suggestions to this work. The detailed referee reports by Sarah Noble and an anonymous referee were greatly appreciated. D.N.'s work was supported by the internal Grant no. R9361 of the Southwest Research Institute and by the NASA's Planetary Geology and Geophysics program, contract no. NAG513038. Funding for the creation and distribution of the SDSS Archive has been provided by the Alfred P. Sloan Foundation, the Participating Institutions, the National Aeronautics and Space Administration, the National Science Foundation, the U.S. Department of Energy, the Japanese Monbukagakusho, and the Max Planck Society. The SDSS Web site is http://www.sdss.org/.

References

Asphaug, E., 1997. New views of asteroids. Science 278, 2070–2071.

Bell, J.F., 20 colleagues, 2002. Near-IR reflectance spectroscopy of 433 Eros from the NIS instrument on the NEAR mission. I. Low phase angle observations. Icarus 155, 119–144.

Bendjoya, P., Zappalà, V., 2002. Asteroid family identification. In: Bottke, W.F., Cellino, A., Paolicchi, P., Binzel, R. (Eds.), Asteroids III. Univ. of Arizona Press, Tucson, pp. 613–618.

Binzel, R.P., Bus, S.J., Burbine, T.H., 1998. Relating S-asteroids and ordinary chondrite meteorites: the new big picture. Bull. Am. Astron. Soc. 30, 1041.

Binzel, R.P., Harris, A.W., Bus, S.J., Burbine, T.H., 2001. Spectral properties of near-Earth objects: Palomar and IRTF results for 48 objects including spacecraft targets (9969) Braille and (10302) 1989 ML. Icarus 151, 139–149.

Binzel, R.P., Lupishko, D., di Martino, M., Whiteley, R.J., Hahn, G.J., 2002. Physical properties of near-Earth objects. In: Bottke, W.F., Cellino, A., Paolicchi, P., Binzel, R. (Eds.), Asteroids III. Univ. of Arizona Press, Tucson, pp. 255–271.

Binzel, R.P., Rivkin, A.S., Stuart, J.S., Harris, A.W., Bus, S.J., Burbine, T.H., 2004. Observed spectral properties of near-Earth objects: results for population distribution, source regions, and space weathering processes. Icarus 170, 259–294.

Bottke, W.F., Vokrouhlický, D., Brož, M., Nesvorný, D., Morbidelli, A., 2001. Dynamical spreading of asteroid families via the Yarkovsky effect. Science 294, 1693–1696.

Bottke, W.F., Morbidelli, A., Jedicke, R., Petit, J., Levison, H.F., Michel, P., Metcalfe, T.S., 2002. Debiased orbital and absolute magnitude distribution of the near-Earth objects. Icarus 156, 399–433.

Bowell, E., Muinonen, K., Wasserman, L.H., 1994. A public-domain asteroid orbit database. In: Milani, A., Di Martino, M., Cellino, A. (Eds.), Asteroids, Comets and Meteors. Kluwer, Dordrecht, pp. 477–481.

Bus, S.J., 1999. Compositional structure in the asteroid belt: results of a spectroscopic survey. PhD thesis.

Bus, S.J., Binzel, R.P., 2002a. Phase II of the small main-belt asteroid spectroscopic survey: the observations. Icarus 158, 106–145.

Bus, S.J., Binzel, R.P., 2002b. Phase II of the small main-belt asteroid spectroscopic survey: a feature-based taxonomy. Icarus 158, 146–177.

Carruba, V., Burns, J.A., Bottke, W., Nesvorný, D., 2003. Orbital evolution of the Gefion and Adeona asteroid families: close encounters with massive asteroids and the Yarkovsky effect. Icarus 162, 308–327.

Cassidy, W., Hapke, B., 1975. Effects of darkening processes on surfaces of airless bodies. Icarus 25, 371–383.

Cellino, A., Zappalà, V., Doressoundiram, A., di Martino, M., Bendjoya, P., Dotto, E., Migliorini, F., 2001. The puzzling case of the Nysa–Polana family. Icarus 152, 225–237.

Cellino, A., Bus, S.J., Doressoundiram, A., Lazzaro, D., 2002. Spectroscopic properties of asteroid families. In: Bottke, W.F., Cellino, A., Paolicchi, P., Binzel, R. (Eds.), Asteroids III. Univ. of Arizona Press, Tucson, pp. 633–643.

Chapman, C.R., 2004. Space weathering of asteroid surfaces. Annu. Rev. Earth Planet. Sci. In press.

Chapman, C.R., Salisbury, J.W., 1973. Comparisons of meteorite and asteroid spectral reflectivities. Icarus 19, 507–522.

Chapman, C.R., Ryan, E.V., Merline, W.J., Neukum, G., Wagner, R., Thomas, P.C., Veverka, J., Sullivan, R.J., 1996. Cratering on Ida. Icarus 120, 77–86.

Chesley, S.R., Ostro, S.J., Vokrouhlický, D., Čapek, D., Giorgini, J.D., Nolan, M.C., Margot, J., Hine, A.A., Benner, L.A.M., Chamberlin, A.B., 2003. Direct detection of the Yarkovsky effect by radar ranging to Asteroid 6489 Golevka. Science 302, 1739–1742.

Clark, B.E., Veverka, J., Helfenstein, P., Thomas, P.C., Bell, J.F., Harch, A., Robinson, M.S., Murchie, S.L., McFadden, L.A., Chapman, C.R., 1999. NEAR photometry of Asteroid 253 Mathilde. Icarus 140, 53–65.

Clark, B.E., 11 colleagues, 2001. Space weathering on Eros: constraints from albedo and spectral measurements of Psyche crater. Meteorit. Planet. Sci. 36, 1617–1637.

Clark, B.E., Hapke, B., Pieters, C., Britt, D., 2002a. Asteroid space weathering and regolith evolution. In: Bottke, W.F., Cellino, A., Paolicchi, P., Binzel, R. (Eds.), Asteroids III. Univ. of Arizona Press, Tucson, pp. 585–599.

Clark, B.E., Helfenstein, P., Bell, J.F., Peterson, C., Veverka, J., Izenberg, N.I., Domingue, D., Wellnitz, D., McFadden, L., 2002b. NEAR infrared spectrometer photometry of Asteroid 433 Eros. Icarus 155, 189–204.

Davis, D.R., Durda, D.D., Marzari, F., Campo Bagatin, A., Gil-Hutton, R., 2002. Collisional evolution of small-body populations. In: Bottke, W.F., Cellino, A., Paolicchi, P., Binzel, R. (Eds.), Asteroids III. Univ. of Arizona Press, Tucson, pp. 545–558.

Dell'Oro, A., Bigongiari, G., Paolicchi, P., Cellino, A., 2004. Asteroid families: evidence of aging of the proper elements. Icarus 169, 341–356.

Doressoundiram, A., Barucci, M.A., Fulchignoni, M., Florczak, M., 1998. EOS family: a spectroscopic study. Icarus 131, 15–31.

Durda, D.D., Dermott, S.F., 1997. The collisional evolution of the asteroid belt and its contribution to the zodiacal cloud. Icarus 130, 140–164.

Fukugita, M., Ichikawa, T., Gunn, J.E., Doi, M., Shimasaku, K., Schneider, D.P., 1996. The Sloan Digital Sky Survey photometric system. Astron. J. 111, 1748.

Gaffey, M.J., Burbine, T.H., Piatek, J.L., Reed, K.L., Chaky, D.A., Bell, J.F., Brown, R.H., 1993. Mineralogical variations within the S-type asteroid class. Icarus 106, 573–602.

Gaffey, M.J., Cloutis, E.A., Kelley, M.S., Reed, K.L., 2002. Mineralogy of asteroids. In: Bottke, W.F., Cellino, A., Paolicchi, P., Binzel, R. (Eds.), Asteroids III. Univ. of Arizona Press, Tucson, pp. 183–204.

Gold, T., 1955. The lunar surface. Mon. Not. R. Astron. Soc. 115, 585–604.

Hapke, B., 2001. Space weathering from Mercury to the asteroid belt. J. Geophys. Res. 106, 10039–10074.

Hirayama, K., 1918. Groups of asteroids probably of common origin. Astron. J. 31, 185–188.

Ivezić, Ž., 32 colleagues, 2001. Solar System objects observed in the Sloan Digital Sky Survey commissioning data. Astron. J. 122, 2749–2784.

Ivezić, Ž., Lupton, R.H., Jurić, M., Tabachnik, S., Quinn, T., Gunn, J.E., Knapp, G.R., Rockosi, C.M., Brinkmann, J., 2002. Color confirmation of asteroid families. Astron. J. 124, 2943–2948.

Ivezić, Ž., 13 colleagues, 2003. Variability Studies with SDSS. Memorie della Societa Astronomica Italiana 74, 978.

Jedicke, R., Nesvorný, D., Whiteley, R., Ivezić, Ž., Jurić, M., 2004. An age–color relationship for main belt S-complex asteroids. Nature 429, 275–277.

Johnson, T.V., Fanale, F.P., 1973. Optical properties of carbonaceous chondrites and their relationship to asteroids. J. Geophys. Res. 78, 8507–8518.

Jurić, M., 15 colleagues, 2002. Comparison of positions and magnitudes of asteroids observed in the Sloan Digital Sky Survey with those predicted for known asteroids. Astron. J. 124, 1776–1787.

Keil, K., 2002. Geological history of Asteroid 4 Vesta: the "smallest terrestrial planet." In: Bottke, W.F., Cellino, A., Paolicchi, P., Binzel, R. (Eds.), Asteroids III. Univ. of Arizona Press, Tucson, pp. 573–584.

Knežević, Z., Lemaître, A., Milani, A., 2002. The determination of asteroid proper elements. In: Bottke, W.F., Cellino, A., Paolicchi, P., Binzel, R. (Eds.), Asteroids III. Univ. of Arizona Press, Tucson, pp. 603–612.

Marzari, F., Davis, D., Vanzani, V., 1995. Collisional evolution of asteroid families. Icarus 113, 168–187.

Marzari, F., Farinella, P., Davis, D.R., 1999. Origin, aging, and death of asteroid families. Icarus 142, 63–77.

McCord, T.B., Adams, J.B., Johnson, T.V., 1970. Asteroid Vesta: spectral reflectivity and compositional implications. Science 178, 745–747.

McFadden, L.A., Wellnitz, D.D., Schnaubelt, M., Gaffey, M.J., Bell, J.F., Izenberg, N., Murchie, S., Chapman, C.R., 2001. Mineralogical interpretation of reflectance spectra of Eros from NEAR near-infrared spectrometer low phase flyby. Meteorit. Planet. Sci. 36, 1711–1726.

McSween, H.Y., 1999. Meteorites and Their Parent Planets. Cambridge Univ. Press, Cambridge, NY.

Michel, P., Tanga, P., Benz, W., Richardson, D.C., 2002. Formation of asteroid families by catastrophic disruption: simulations with fragmentation and gravitational reaccumulation. Icarus 160, 10–23.

Michel, P., Benz, W., Richardson, D.C., 2003. Disruption of fragmented parent bodies as the origin of asteroid families. Nature 421, 608–611.

Migliorini, F., Michel, P., Morbidelli, A., Nesvorný, D., Zappalà, V., 1998. Origin of multikilometer Earth- and Mars-crossing asteroids: a quantitative simulation. Science 281, 2022–2024.

Milani, A., Farinella, P., 1994. The age of the Veritas asteroid family deduced by chaotic chronology. Nature 370, 40–41.

Milani, A., Knežević, Z., 1994. Asteroid proper elements and the dynamical structure of the asteroid main belt. Icarus 107, 219–254.

Morbidelli, A., Vokrouhlický, D., 2003. The Yarkovsky-driven origin of near-Earth asteroids. Icarus 163, 120–134.

Murchie, S., 10 colleagues, 2002. Color variations on Eros from NEAR multispectral imaging. Icarus 155, 145–168.

Nesvorný, D., Bottke, W.F., 2004. Detection of the Yarkovsky effect for main-belt asteroids. Icarus 170, 324–342.

Nesvorný, D., Bottke, W.F., Dones, L., Levison, H.F., 2002a. The recent breakup of an asteroid in the main-belt region. Nature 417, 720–771.

Nesvorný, D., Morbidelli, A., Vokrouhlický, D., Bottke, W.F., Brož, M., 2002b. The Flora family: a case of the dynamically dispersed collisional swarm? Icarus 157, 155–172.

Nesvorný, D., Bottke, W.F., Levison, H.F., Dones, L., 2003. Recent origin of the Solar System dust bands. Astrophys. J. 591, 486–497.

Noble, S.K., Pieters, C.M., Keller, L.P., 2004. Quantitative aspects of space weathering: implications for regolith breccia meteorites and asteroids. Lunar. Planet. Sci. Conf. 35, 1301–1303.

Pieters, C.M., Taylor, L.A., Noble, S.K., Keller, L.P., Hapke, B., Morris, R.V., Allen, C.C., McKay, D.S., Wentworth, S., 2000. Space weathering on airless bodies: resolving a mystery with lunar samples. Meteorit. Planet. Sci. 35, 1101–1107.

Press, W.H., Teukolsky, S.A., Vetterling, W.T., Flannery, B.P., 1992. Numerical Recipes in C: The Art of Scientific Computing. Cambridge Univ. Press, Cambridge, NY.

Rabinowitz, D.L., 1998. NOTE: Size and orbit dependent trends in the reflectance colors of Earth-approaching asteroids. Icarus 134, 342–346.

Richardson, D.C., Bottke, W.F., Love, S.G., 1998. Tidal distortion and disruption of Earth-crossing asteroids. Icarus 134, 47–76.

Rivkin, A.S., Davies, J.K., Johnson, J.R., Ellison, S.L., Trilling, D.E., Brown, R.H., Lebofsky, L.A., 2003. Hydrogen concentrations on C-class asteroids derived from remote sensing. Meteorit. Planet. Sci. 38, 1383–1398.

Roush, T.L., Singer, R.B., 1984. Modelling of temperature effects on spectral reflectance of asteroid surfaces. Bull. Am. Astron. Soc. 16, 710.

Sasaki, S., Nakamura, K., Hamabe, Y., Kurahashi, E., Hiroi, T., 2001. Production of iron nanoparticles by laser irradiation in a simulation of lunar-like space weathering. Nature 410, 555–557.

Sasaki, T., 9 colleagues, 2004. Mature and fresh surfaces on new-born Asteroid Karin. Nature. Submitted for publication.

Shingareva, T.V., Basilevsky, A.T., Fisenko, A.V., Semjonova, L.F., Roshchina, I.A., Guseva, E.V., Korotaeva, N.N., 2003. Mineralogy and petrology of laser irradiated artificial carbonaceous chondrite: implication to the martian moons and some asteroids. Proc. Lunar Planet. Sci. Conf. 34, 1321–1323.

Stoughton, C., 191 colleagues, 2002. Sloan Digital Sky Survey: early data release. Astron. J. 123, 485–548.

Sullivan, R., 17 colleagues, 1996. Geology of 243 Ida. Icarus 120, 119–139.

Sullivan, R.J., Thomas, P.C., Murchie, S.L., Robinson, M.S., 2002. Asteroid geology from Galileo and NEAR Shoemaker data. In: Bottke, W.F., Cellino, A., Paolicchi, P., Binzel, R. (Eds.), Asteroids III. Univ. of Arizona Press, Tucson, pp. 331–350.

Sykes, M.V., Cutri, R.M., Fowler, J.W., Tholen, D.J., Skrutskie, M.F., Price, S., Tedesco, E.F., 2000. The 2MASS asteroid and comet survey. Icarus 146, 161–175.

Tanga, P., Cellino, A., Michel, P., Zappalà, V., Paolicchi, P., dell'Oro, A., 1999. On the size distribution of asteroid families: the role of geometry. Icarus 141, 65–78.

Tedesco, E.F., Noah, P.V., Noah, M., Price, S.D., 2002. The supplemental IRAS minor planet survey. Astron. J. 123, 1056–1085.

Veverka, J., 11 colleagues, 1996. Ida and Dactyl: spectral reflectance and color variations. Icarus 120, 66–76.

Veverka, J., 13 colleagues, 1999. NEAR Encounter with Asteroid 253 Mathilde: overview. Icarus 140, 3–16.

Veverka, J., 32 colleagues, 2000. NEAR at Eros: imaging and spectral results. Science 289, 2088–2097.

Vokrouhlický, D., 1999. A complete linear model for the Yarkovsky thermal force on spherical asteroid fragments. Astron. Astrophys. 344, 362–366.

Whiteley, R.J., 2001. A compositional and dynamical survey of the near-Earth asteroids. PhD thesis. University of Hawaii, pp. 202.

Xu, S., Binzel, R.P., Burbine, T.H., Bus, S.J., 1995. Small main-belt asteroid spectroscopic survey: initial results. Icarus 115, 1–35.

Yoshida, F., 8 colleagues, 2004. Photometric Observation of Karin Family Asteroids, Asteroid Dynamics Workshop, February 2–4. Arecibo Observatory, Arecibo, Puerto-Rico.

Zappalà, V., Cellino, A., Farinella, P., Knežević, Z., 1990. Asteroid families. I. Identification by hierarchical clustering and reliability assessment. Astron. J. 100, 2030–2046.

Zappalà, V., Cellino, A., Farinella, P., Milani, A., 1994. Asteroid families. 2. Extension to unnumbered multiopposition asteroids. Astron. J. 107, 772–801.

Zappalà, V., Bendjoya, P., Cellino, A., Farinella, P., Froeschle, C., 1995. Asteroid families: search of a 12,487-asteroid sample using two different clustering techniques. Icarus 116, 291–314.